Nature-Inspired, Computer-Assisted Optimization of Hierarchically Structured Zeolites

Marc-Olivier Coppens[*1], Tobias Weissenberger[1], Qunfeng Zhang[2] and Guanghua Ye[2]*

Prof. Marc-Olivier Coppens, Dr. Tobias Weissenberger

Department of Chemical Engineering and Centre for Nature-Inspired Engineering, University College London, London WC1E 7JE, United Kingdom

E-mail: m.coppens@ucl.ac.uk

Qunfeng Zhang, Prof. Guanghua Ye

State Key Laboratory of Chemical Engineering, School of Chemical Engineering, East China University of Science and Technology, Shanghai 200237, China

E-mail: guanghuaye@ecust.edu.cn

Keywords: zeolites, diffusion, catalysis, nature-inspired, surface barriers

Abstract

Zeolite catalysis is often affected by transport limitations, which significantly influence overall performance. Introducing wide pores as molecular transport highways can reduce transport limitations, control the product distribution, and mitigate effects of catalyst deactivation. Nevertheless, the importance to rationally design the meso- and macropore space remains underappreciated. This article reviews multiscale modelling approaches to optimize overall catalytic performance. It provides a general methodology and rules of thumb to guide catalyst synthesis with optimal pore network characteristics. Inspiration is taken from nature, such as the structure of leaves and tissues, with similar requirements and associated

features. In optimal hierarchically structured zeolites, the added macro-/mesopore volume fraction, connectivity, crystal size and minimum wide pore size are crucial. The broad pore size distribution is secondary. No uncontrolled diffusion limitations should exist within the zeolite crystals. Surface barriers, however, can significantly affect, even dominate overall transport. Understanding their origin and ways to control them is an emergent research area. Synthesis methods to realize hierarchically structured zeolites are briefly reviewed. Significant gaps exist between laboratory synthesis methods and industrial requirements. Zeolite catalysis could benefit from computer-assisted design of their hierarchical pore network, embracing principles used by natural transport networks for scalable efficiency, selectivity and robustness.

1. Introduction

Molecular transport networks are essential to life. Here, we discuss how their structural features, optimized over the eons, may guide the design of more efficient and robust porous catalyst architectures. Although the principles are more general, we illustrate this for zeolites, a very important class of microporous catalysts, where transport limitations are common and significantly influence product yields, product distributions and catalyst stability.

From fertile river deltas to tree crowns, from the vascular network to the pulmonary architecture: scalable networks in nature carry molecules to and from sites where the "action" occurs. This action involves exchange processes and reactions, from the cellular level down to the nano- and the molecular scale. A closer look reveals that the architecture of many such transport networks, in all their outward disparity, bears universal features – especially when transport is a limiting step, and is essential to preserve function, irrespective of scale. At macroscopic scales, natural branching architectures are self-similar fractals over a range of magnifications.[1] This is observed in tree crowns, root networks or the airway tree of the lungs, where a repeatedly branching, fractal architecture bridges a wide range, and allows these networks to grow, all while preserving the function at a cellular level. At macroscopic scales, gaseous and liquid transport mechanisms include convective flow, driven by pressure differences, and, for liquid flow in narrower channels, capillary action. A self-similar architecture leads to equivalent hydraulic pathlengths, between a source (stem) or drain (collection) and a multitude of sites that are distributed over space and can cover a vast surface area.[2] The dominant transport mechanism at mesoscopic to microscopic scales is typically diffusion; despite the random molecular motion, concentration or chemical potential gradients drive the transport of individual species to and from the active sites, where adsorption, reaction and desorption occur. Interestingly, the structural features of natural

networks are different at this scale: they tend to be much more uniform and interconnected. These characteristics are observed in leaves, the alveolar sacs or tissues crisscrossed by fine blood capillaries.

For porous catalyst design, guidance from such transport networks in nature could serve to achieve similarly efficient and robust species transport.[3] This should be obtained, not by simply imitating their *apparent* features, but by learning from the aforementioned universal, physical *mechanisms* that underpin optimal transport networks, and then implement these network properties in nature-inspired designs. This requires a deeper investigation on how structural features relate to different transport properties at all scales, while appreciating the different context and design constraints in nature and in applied catalysis. Nature-inspired designs are further refined by computer-assisted optimization. Their translation to practice integrates advances in materials synthesis. There has been tremendous progress in the synthesis of zeolite-based materials, with controlled crystal shapes, sizes and organization into architectures of ever-expanding variety.[4] However, the question is which architecture is best for a particular application in catalysis? Are there common features, and parameters that matter more than other ones, related to the organization of the pore space, the size of the crystallites and the distance between them? In addition, it has become increasingly clear that not only transport inside the microporous zeolite crystals (intracrystalline diffusion), or even via the traversing or embedding network of meso- and macropores within a catalyst particle or pellet could be transport limiting, but that transport across the crystal facets may well become the rate limiting step.[5] This means that either the external crystal surface, or the internal surfaces in polycrystalline samples could be formidable “surface barriers” that dominate the overall, observed transport and catalytic rates.[6]

In this article we will discuss the rapidly progressing subject of hierarchically structured zeolites from a distinctive angle that, we hope, may serve as a guiding principle for better

catalyst designs. This angle relies on the application of a systematic nature-inspired solution methodology, in the context of nature-inspired chemical engineering (NICE).[7] This methodology is assisted by computation, which informs the desired pore network architecture and synthesis parameters.

First, in Section 2, we will briefly review some basic concepts of diffusion and reaction in porous catalysts: how to quantify the significance of diffusion limitations, how to model diffusion at multiple scales, and how diffusion and reaction can be modeled in hierarchically structured, zeolite-based porous catalysts, including micro-, meso- and macropores. This overview is not meant to be exhaustive, but simply to serve as a guide for chemists and materials scientists and as a refresher for chemical engineers.

Then, in Section 3, we discuss the nature-inspired solution methodology, as applied to hierarchical, porous catalyst design. In Section 4, we succinctly review different methods to synthesize hierarchically structured zeolites, summarizing suitable pathways to realize the nature-inspired designs for porous catalyst architectures with optimized properties. We will also see how comparing experiments with computational optimization results has revealed that both external and internal zeolite surface barriers may come into play. This sets the scene for the next challenge, to design surface barriers, where, as part of the conclusions and outlook in Section 5, we argue that lessons from nature could be learnt, once again.

2 Diffusion and reaction in porous catalysts

2.1 Diffusion limitations

In a porous catalyst particle, besides surface reactions, diffusion takes place. Together, they constitute the overall, observed catalytic process. Figure 1 shows schematically how reactants must diffuse a distance ranging from nanometers to millimeters, before reaching an active site on the internal surface of a porous catalyst particle and then undergoing surface

reactions. Products formed on the active site thus need to diffuse from the active sites to the external surface of the catalyst, before being carried away in the flowing fluid. When the time required for diffusion is important, compared to that of surface reaction, diffusion becomes a limiting step that strongly affects the apparent reaction rates. According to Einstein[8], the diffusion time, t_d, of a molecule is given by:

$$t_d = \frac{\left\langle \left| \mathbf{r}(t) \right|^2 \right\rangle}{6D} \qquad (1),$$

where $\left\langle \left| \mathbf{r}(t) \right|^2 \right\rangle$ is the mean square displacement of the molecule, and D is the (self-)diffusion coefficient. As Eq. (1) shows, the diffusion time is proportional to the square of the end-to-end distance, so that diffusion limitations may become significant for porous catalyst particles used in practice, when their particle size is large. For completeness, Einstein's formula only holds for isotropic random walks in which the steps are not strongly correlated in space or in time. Eq. (1) also does not hold when the individual steps in the random walk follow a distribution with infinite variance. In such cases, the central limit theorem no long holds, and diffusion becomes anomalous;[1, 8] then, time, t_d, needs to be replaced by another function, often a power law, $(t_d)^\alpha$, where $0 < \alpha < 1$ for sub-diffusion, $\alpha > 1$ for super-diffusion, and D needs to be replaced by a generalized diffusion coefficient. Eq. (1) holds for normal diffusion, $\alpha = 1$, which is the case in all examples in this article. However, a special case relevant to certain zeolites is single-file diffusion in long, one-dimensional channels, where molecules cannot pass each other; in this case, $\alpha = 0.5$.[9]

In industry, the catalyst particle size cannot be reduced at will, as catalysts must meet various engineering requirements, such as limiting the pressure drop in fixed bed reactors, sufficient mechanical strength, or the need to separate catalyst particles from products; all are critical for the successful use of a catalyst in an industrial reactor.[10] In addition, the diffusion time is proportional to the inverse of the diffusivity, which is an intrinsic physical property in the bulk.

However, in a porous catalyst, the diffusion of a substance is confined to the typically very narrow pores, and the interactions between molecules and pore wall can exert strong influences on the diffusion process. For zeolites, due to the confinement of their micropores (diameters less than 2 nm), the diffusivity of a substance can be as low as 10^{-9}-10^{-18} m^2/s, which is typically 4-10 orders of magnitude smaller than the diffusivity in the bulk phase.[11] Thus, diffusion limitations can still persist in zeolite catalysts, even if the diffusion path length is reduced down to several nanometers.[12] The overall diffusivity, accounting for the various restrictions of porous materials on the diffusion of guest molecules, is called the effective diffusivity, and is denoted by D_{eff}.

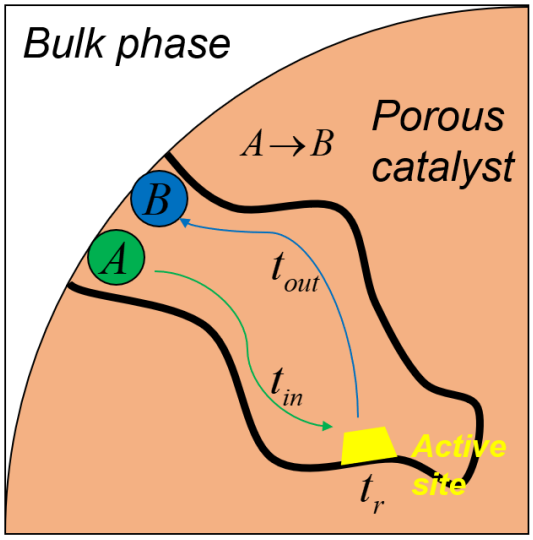

Figure 1. Schematic illustration of diffusion and reaction in a porous catalyst particle. For the sake of simplicity, the reaction is indicated as A→B, with an intrinsic reaction time, t_r. The diffusion time for A diffusing from the external surface to an active site on the internal surface is t_{in}, while that for B diffusing from the active site to the external surface is t_{out}.

In chemical reaction engineering, the effectiveness factor, η, is introduced to quantify the effects of diffusion limitations on the apparent, overall activity of a porous catalyst at the particle or pellet scale. It is defined as the ratio of the observed reaction rate of a catalyst, which includes the influence of diffusion limitations, to the intrinsic reaction rate, when the

catalyst is assumed to bathe in the external surface conditions:[13]

$$\eta = \frac{observed\ rate\ of\ reaction}{rate\ of\ reaction\ at\ external\ surface\ conditions} \qquad (2).$$

For a first-order irreversible reaction, the effectiveness factor is:

$$\eta(\phi) = \begin{cases} \dfrac{tanh(\phi)}{\phi} & for\ a\ slab \\ \dfrac{2I_1(\phi)}{\phi I_0(\phi)} & for\ a\ cylinder \\ \dfrac{3}{\phi}\left[\dfrac{1}{tanh(\phi)} - \dfrac{1}{\phi}\right] & for\ a\ sphere \end{cases} \qquad (3).$$

Here, ϕ is the Thiele modulus:

$$\phi = L\sqrt{\frac{k}{D_{eff}}} \qquad (4),$$

and its square can be considered as the ratio of the characteristic time for diffusion (t_d) to that for reaction (t_r):

$$\phi^2 = \frac{kL^2}{D_{eff}} = \frac{t_d}{t_r} \qquad (5),$$

$$L = \frac{V}{A} \qquad (6),$$

where k is the reaction rate constant, L is the characteristic length of the catalyst particle, D_{eff} is the effective diffusivity, and V and A are the volume and external surface area of the catalyst particle, respectively. In Eq. (3), $I_0(\phi)$ and $I_1(\phi)$ are modified Bessel functions of the first kind. Figure 2 shows the relation between effectiveness factor and Thiele modulus for slab-like, cylindrical and spherical catalyst particles. For an intrinsically slow reaction, where $t_d \ll t_r$, the Thiele modulus $\phi \to 0$ and $\eta \to 1$. However, for strongly diffusion limited reactions, $t_d \gg t_r$, the Thiele modulus $\phi \to \infty$ and $\eta \sim 1/\phi$ for a slab, $\eta \sim 2/\phi$ for a cylinder

and $\eta \sim 3/\phi$ for a sphere. The effectiveness factor decreases when the Thiele modulus increases, due to more significant diffusion limitations. As seen from Eq. (5), a shrinking catalyst particle size and an increasing effective diffusivity decrease the Thiele modulus and, therefore, increase the effectiveness factor. This is also the case for any reaction with kinetics that are of positive reaction order; here, the Thiele modulus, ϕ, should be replaced by a generalized Thiele modulus, Φ, for general kinetics, $r = r(C)$:

$$\Phi = \frac{V}{A}\frac{r(C_0)}{\sqrt{2}}\left[\int_{C_c}^{C_0} D_{eff} r(C)\, dC\right]^{-1/2} \qquad (7).$$

Here, C_0 is the concentration of the key reactant at the external catalyst surface and C_c is its concentration in the center of the pellet, where it is often assumed to be zero, which is only strictly correct for strongly diffusion limited reactions.

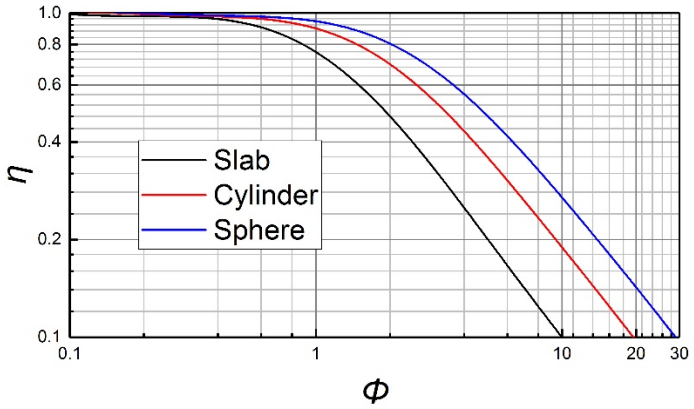

Figure 2. The relation between Thiele modulus, $\boldsymbol{\phi}$, and effectiveness factor, η, for a first-order irreversible reaction in a slab, cylindrical and spherical catalyst particle.

Decreasing the particle size or increasing the effective diffusivity by improving the pore network structure are two approaches that can be used to effectively enhance the apparent reaction rate observed for a porous catalyst particle, without changing the structure of the active phase. For zeolite catalysts, the two approaches are widely used to improve the apparent catalytic activity. For example, Ye et al.[14] probed the influence of particle size on the apparent activity of Pt/Beta zeolite for catalyzing *n*-pentane isomerization. They found

that the observed turnover frequency (TOF) decreases from 1.44 to 0.74 s^{-1} when the particle size increases from 250 to 1340 nm at the reaction temperature of 653 K, and they attributed this observation to the lengthened diffusion path. Fernandez et al.[15] prepared ZSM-5 zeolite catalysts with a mesoporous-microporous structure for catalyzing isomerization of *o*-xylene, and the results show that the hierarchical ZSM-5 is far more active than the purely microporous ZSM-5.

Diffusion limitations also play an important role in affecting the selectivity towards various products, when there are parallel or consecutive reactions.[13, 16] The instantaneous selectivity toward desired product, D, with respect to undesired product, U, is defined as the ratio of the production rate of D to that of U:[17]

$$S_{D/U} = \frac{\text{rate of formation of D}}{\text{rate of formation of U}} = \frac{r_D}{r_U} \qquad (8).$$

In porous catalysts, diffusion limitations can affect the selectivity through changing the apparent (and not just the intrinsic) reaction rates of different substances. The diffusivity of a substance is highly dependent on its physicochemical and geometrical properties (e.g., molecular weight and size), resulting in different diffusivities for different substances. In addition, the pore network structure can have a different effect on the diffusion rate of various components. The combined differences in effective diffusivity can lead to distinct apparent formation rates of products and, thus, distinct selectivities and product distributions. For zeolite catalysts, the effects of diffusion on selectivity can be very important, as the micropores are barely wider than the molecules; therefore, a slight change in molecular properties can result in a significant change in molecule-wall interactions and, consequently, a strong influence on the diffusivity. Based on this phenomenon, zeolite catalysts can be engineered to tune selectivity towards desired products; in particular, molecular geometry affects size- and shape-selectivity. For instance, Chen et al.[18] studied the shape-selective catalysis of ZSM-5 zeolite for the alkylation of toluene with methanol. They found that the

product distribution is close to thermodynamic equilibrium when the crystal size is less than 0.5 μm, while the production of *p*-xylene exceeds its equilibrium yield when the crystal size increases to 3 μm. The diffusion of *p*-xylene is faster than diffusion of *o*- and *m*-xylene, and this effect becomes more obvious for an increased diffusion path length.

Diffusion limitations also affect catalyst stability. Catalyst deactivation is a common and complex phenomenon that can be caused by poisoning, fouling, thermal degradation (e.g., sintering, evaporation), mechanical damage, and corrosion or leaching.[19] Reactants, intermediates, and products could all be involved in the deactivation of a porous catalyst particle. Among these causes, deactivation by fouling is encountered in most catalytic processes. During reactions, some high-boiling byproducts (e.g., coke) can be formed, and they accumulate in the catalyst particle if the desired products are unable to diffuse out in time. Besides, diffusion limitations also affect the formation rate of the high-boiling byproducts by changing the concentration profiles of the intermediates of these byproducts in the catalyst particle.[20] These high-boiling byproducts can cover the active sites and, thus, directly reduce the number of available active sites. With the accumulation of these byproducts on the pore walls, the pores can become narrow and even plugged, which further deteriorates diffusion and considerably reduces the accessibility of the active sites. For zeolite catalysts, the effect of diffusion on catalyst lifetime can be even more obvious, since micropores can be easily plugged by high-boiling byproducts. For example, Kim et al.[21] synthesized hierarchically structured Zn/ZSM-5 to catalyze the aromatization of branched olefins, and they found that a hierarchical microporous-mesoporous structure can dramatically prolong the catalyst lifetime. They explained that introducing the hierarchical pore structure can enhance the tolerance to coking, and it also allows coke precursors to diffuse quickly, so that they can escape from the micropores, before being converted into coke and then plugging these pores.

2.2 Multiscale transport in zeolite-based catalysts and processes

A typical porous catalyst usually contains a hierarchical transport network, in which diffusion over multiple scales occurs.[4d, 16b] Let us take a fixed-bed reactor, packed with zeolite catalyst pellets, as an example to illustrate the hierarchical transport network and the multiscale transport (Figure 3). At the reactor scale (macroscale), the interparticle voids provide the space for mass transfer. Although diffusion takes place in the voids, convection is the dominant mass transfer mechanism. At the catalyst particle scale (mesoscale), diffusion typically becomes the principal mass transfer mechanism. This diffusion can be subdivided into molecular diffusion, Knudsen diffusion, surface diffusion, and configurational diffusion, based on the interactions between molecules and pore walls (Figure 4).[22] At the active site scale (microscale), adsorption, surface reactions and desorption take place. Although the surface reaction is the actual step where reactants are converted into products, multiscale transport affects the local physicochemical conditions around these active sites, like the local species concentrations. Thus, the efficiency of multiscale diffusion and other transport phenomena in this catalytic reaction system strongly influences the overall performance of the whole system to produce a particular product distribution.

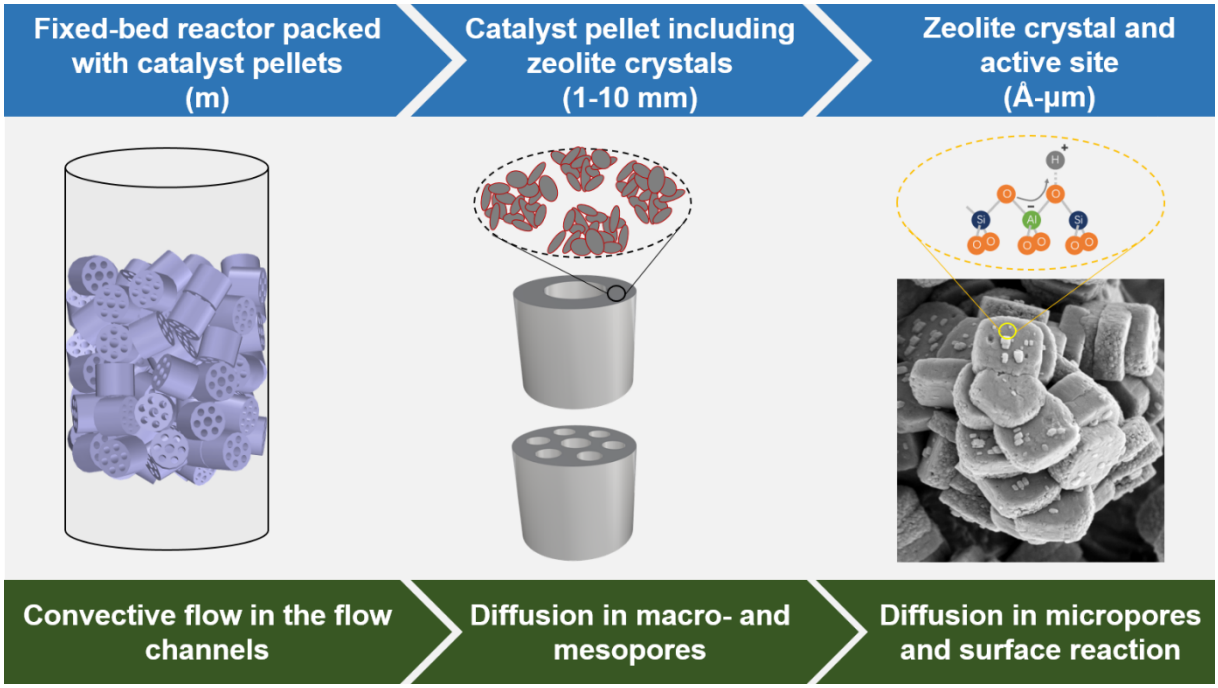

Figure 3. Illustration of the hierarchical, multiscale convective and diffusive transport network in a fixed bed reactor, packed with zeolite catalyst pellets.

Molecular diffusion is usually dominant in macropores (d > 50 nm), especially those wider than a few 100 nm, where the mean free path of a molecule is shorter than the pore size and the frequency of intermolecular collisions is higher than that of molecule-wall collisions. For a binary gas mixture of i and j, the binary molecular diffusivity ($D_{i,j}$) can be calculated using the Chapman-Enskog Equation:[23]

$$D_{i,j} = \frac{3}{16}\frac{\left(4\pi k_B T/M_{ij}\right)^{0.5}}{n\pi\sigma_{ij}^2\Omega_D} f_D \quad (9),$$

$$M_{ij} = \frac{2}{\frac{1}{M_i}+\frac{1}{M_j}} \quad (10),$$

$$\sigma_{ij} = \frac{\sigma_i+\sigma_j}{2} \quad (11),$$

where M_i and M_j are the molecular weights of components i and j, σ_i and σ_j are the characteristic Lennard-Jones length parameters for components i and j, k_B is Boltzmann's constant, T is the absolute temperature, n is the number density of molecules in the mixture, Ω_D is the collision integral for diffusion, and f_D is a correction term that is of the order of unity. If f_D is set to unity and n is determined by the ideal gas law, then Eq. (9) can be written as:

$$D_{i,j} = \frac{0.00266T^{1.5}}{PM_{ij}^{0.5}\sigma_{ij}^2\Omega_D} \quad (12),$$

where P is the pressure. For a multicomponent mixture, the Stefan-Maxwell equations[13, 24] should be used, which relate the molar fluxes to the concentration gradients (or, more correctly, the chemical potential gradients):

$$-\frac{x_i}{RT}\nabla_T \mu_i = \sum_{\substack{j=1 \\ j\neq i}}^{n} \frac{x_j J_i - x_i J_j}{c_t D_{i,j}}, \quad i = 1,2,...,n \qquad (13),$$

where x_i and x_j are the molar fractions of component i and j, J_i and J_j are the diffusion fluxes of component i and j, R is the ideal gas constant, and μ_i is the chemical potential of component i.

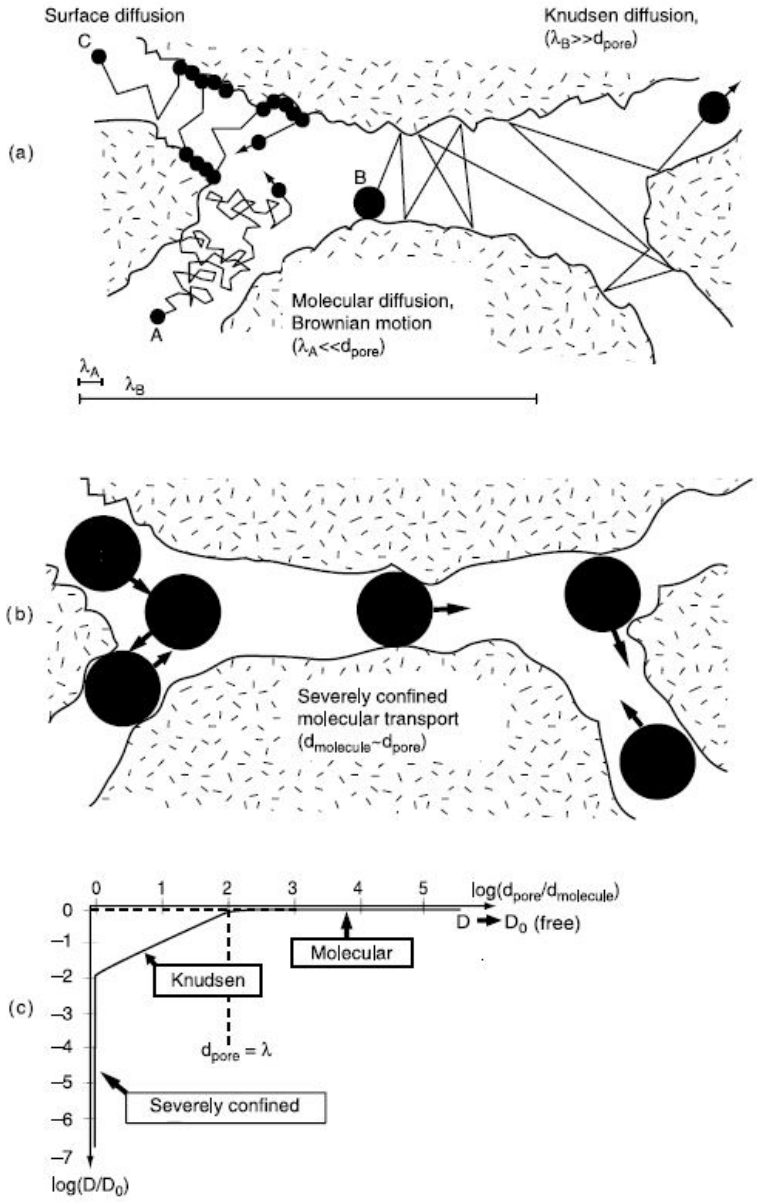

Figure 4. Schematic representation of the different diffusion mechanisms in a porous medium: (a) molecular diffusion, Knudsen diffusion, and surface diffusion; (b) configurational diffusion, which is typical in zeolites; (c) an indication of the different diffusion regimes.[16b] Reprinted with permission from reference 16b. Copyright 2005 Taylor and Francis Group.

For reactions in the gas phase, Knudsen diffusion becomes important in mesopores ($2 < d <$ 50 nm), where molecule-wall collisions significantly affect the movement of molecules. The Knudsen diffusivity of component i ($D_{i,K}$) can be determined as follows, for a long cylindrical pore:

$$D_{i,K} = \frac{d}{3}\sqrt{\frac{8RT}{\pi M_i}} \qquad (14),$$

where d is the pore diameter. When both Knudsen diffusion and molecular diffusion are important, the effective diffusivity of component i ($D_{i,e}$) can be approximated by the Wilke-Bosanquet equation:[25]

$$\frac{1}{D_{i,e}} = \frac{1}{D_{i,m}} + \frac{1}{D_{i,K}} \qquad (15).$$

Surface diffusion describes the movement of adsorbed molecules along pore wall surfaces, and this diffusion mechanism becomes dominant for narrow pores and strongly adsorbed molecules (Figure 4a).[26] In microporous materials, like zeolites, configurational diffusion[27] occurs (Figure 4b); like surface diffusion, this type of diffusion is an activated process, as the effect of the pore walls on the movement of the molecules is very strong.[26, 28] Molecules cannot directly pass each other; in one-dimensional zeolites, this leads to anomalous, single-file diffusion.[9b-e]

In zeolites, the diffusivity is strongly dependent on the molecular loading or occupancy by the adsorbed species. Kärger and Pfeifer[29] have identified several types of loading dependencies for self-diffusion in zeolites, as illustrated in Figure 5. For Type I, the diffusivity is loading-independent when the loading is low enough. For Type II, the diffusivity gradually (e.g., linearly) decreases with loading and approaches a very small value when the zeolite is saturated. Type II is frequently observed, and this can often be explained by the reduction of available volume for diffusion with increased loading. For Type III, the diffusivity first increases with loading, before it decreases to a very small value; this case is found for the

diffusivity of many light gases in cage-like zeolites.[9a, 30] It was shown using kinetic Monte-Carlo simulations that this maximum can arise in zeolites with sites of different adsorption strengths. At low loadings, molecules gradually saturate the strongest adsorption sites, so that other molecules increasingly move along sites that are weaker, and, thus, their diffusion is faster.[30] Beyond a critical loading, crowding in the zeolite pore network lengthens the trajectories, as the strong sites are mostly occupied, so that the overall self-diffusivity decreases again. For Type IV, the diffusivity strongly decreases and reaches a very small value, even when the zeolite is not saturated; this case is found for linear hydrocarbons in zeolite MFI, where two distinct adsorption sites are present in this system.[31]

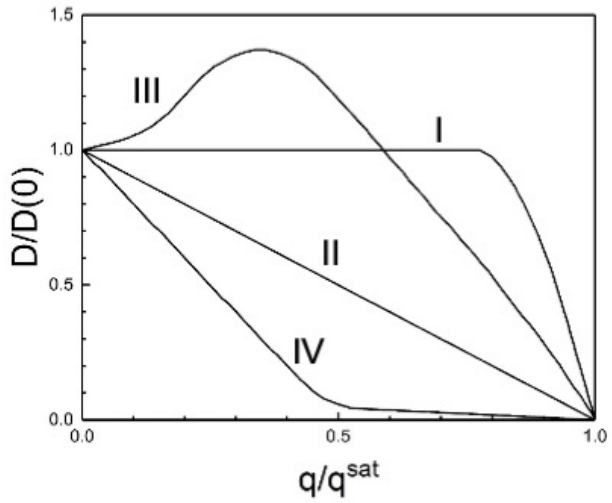

Figure 5. Four types of loading dependencies for self-diffusivity in zeolites; here q is the guest loading and q^{sat} is the loading at saturation (full occupancy). The trends are normalized with respect to the self-diffusivity at zero (or very low) loading.

In zeolite catalysts, in addition to intracrystalline diffusion through the micropores, it has become increasingly clear over the past few years that external surfaces and internal interfaces also create important barriers to molecular transport. They can even become the rate-limiting step for the entire mass transfer process. External and internal diffusion barriers were discovered when studying diffusion in very large zeolite crystals.[5a, 5b, 32] In these studies, experiments with pulsed-field gradient (PFG) NMR, interference microscopy and IR

microscopy were used to measure diffusion in zeolite crystals, and abnormal mass transfer behaviors were observed, such as unusual transient concentration profiles (Figure 6). Such behaviors could only be explained when accounting for the presence of diffusion barriers across crystal faces. For example, for the cases of methanol in ferrierite and SAPO-34 zeolite crystals,[5c, 32a] the concentrations at the internal boundaries of the zeolite crystals are not in equilibrium with the external gas phase during adsorption uptake, which violates a common assumption. A surface permeability (α) has been introduced to relate the flux of a component *i* through the crystal surface (N_i) to the concentration difference over the surface barrier:[33]

$$N_i = \alpha_i \left(C_{i,eq} - C_{i,surf} \right) \quad (16).$$

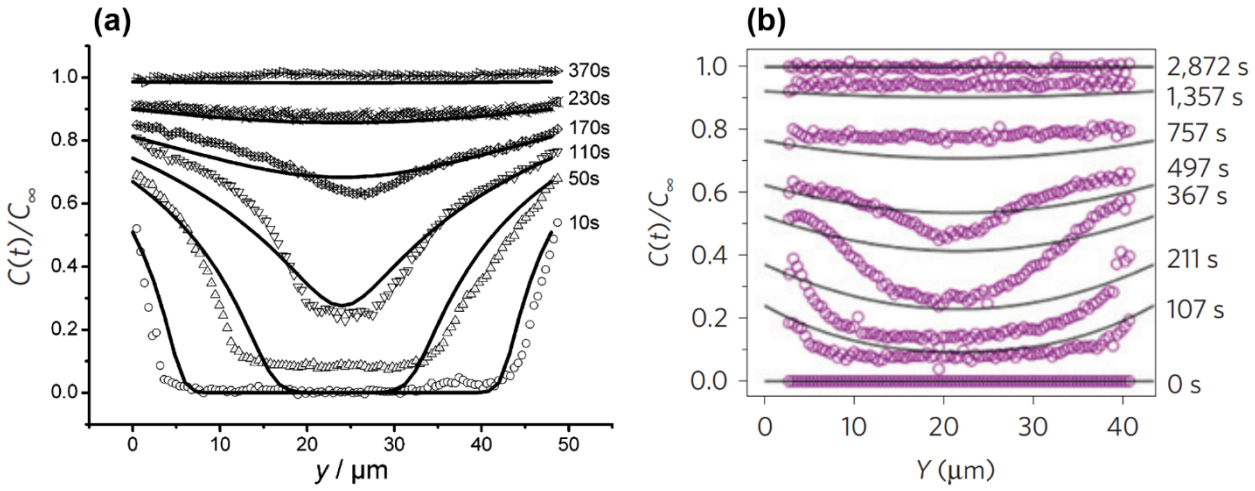

Figure 6. Direct evidence for the existence of diffusion barriers at a zeolite crystal surface. (a) Concentration profiles of methanol in a ferrierite zeolite crystal during transient adsorption experiments;[32b] (b) concentration profiles of methanol in a SAPO-34 zeolite crystal during transient adsorption experiments.[5c] Reprinted with permission from reference 32b. Copyright 2001 American Chemical Society. Reprinted with permission from reference 5c. Copyright 2015 Springer Nature.

2.3 Hierarchical pore structure in zeolite-based catalysts

The void space in a porous catalyst pellet can be ordered or disordered at different length scales. For zeolite-based catalysts, the subject of this review, the intracrystalline void space is periodically ordered. As shown in Figure 7, the catalyst particles or pellets used in practice have a hierarchical structure. They contain zeolite crystals, but possibly also amorphous

components with a different catalytic and/or structural function (e.g., binders), or acting as a diluent to influence the overall transport properties. All of these functions are present in a fluid catalytic cracking (FCC) catalyst particle. In general, there may be one or two levels of hierarchy, as shown in Figure 7. The intra-pellet, inter-crystalline void space consists of mesopores and macropores.

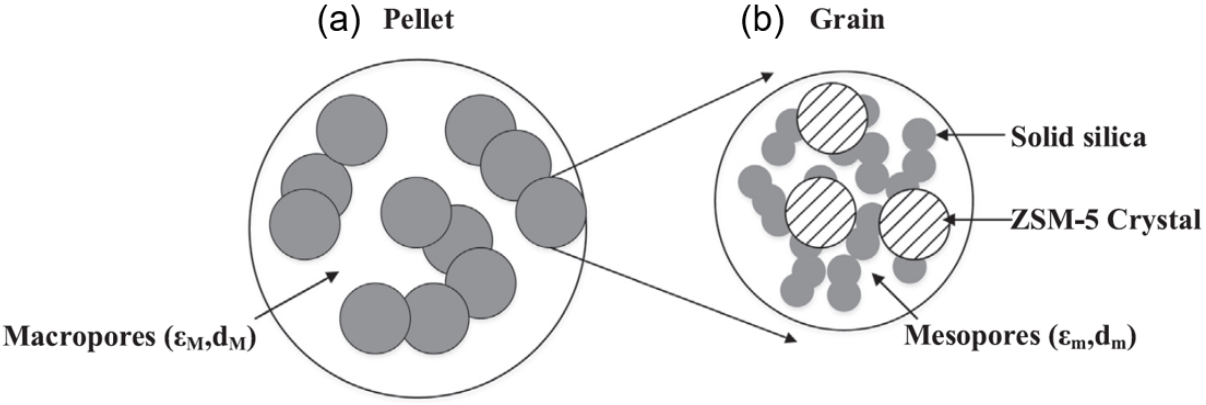

Figure 7. (a) Hierarchically structured pellet, with macropores (porosity, ε_M, and average diameter, d_M) in between (b) grains, which include zeolite crystals (here, ZSM-5) and an additive (here silica nanoparticles), with mesopores (porosity, ε_m, and average diameter, d_m) in between them (after Rao *et al.*).[6a]

As the external shape and size of zeolite crystals are not uniform, the macropores and mesopores formed among these crystals are normally disordered. In contrast, the micropores in zeolite crystals are ordered, although the shape of the micropores and the topology of the micropore network vary for different types of zeolites. It is easier to model ordered transport channels than to model disordered ones. To describe transport in the disordered void space, continuum models and discrete models can be used. Continuum models treat the porous catalyst as a pseudo-homogeneous continuum, while discrete models explicitly account for the pores and their connectivity. These two types of models have been extensively reviewed by Sahimi et al.[34] and Keil.[22a]

Figure 8 illustrates a few archetypical pore models and pore network models. One of the earliest pore models is the parallel pore model developed by Wheeler.[16a] In this model, the

void space is represented by parallel pores of different sizes. The volume-averaged pore radius $\bar{r}$ and length $\bar{L}$ can be calculated by:

$$\bar{r} = \frac{2V_g}{S_g}\sigma(1-\varepsilon) \tag{17}$$

and

$$\bar{L} = \frac{V}{A}\sqrt{2} \tag{18},$$

where V_g is the specific pore volume, S_g is the BET specific internal surface area, σ is the pore wall roughness factor, and ε is the porosity of the catalyst particle. To account for more features of real porous catalysts, other pore models have also been proposed. Some examples of these models include the tortuous pore model,[35] the model of Wakao and Smith,[36] and the grain model.[37] These early models can describe the geometries of the void space in a porous catalyst well, but they fail to account for the pore network connectivity and spatial distribution of the pores.

Pore network models describe the void space using networks of pore channels, which meet each other in intersections.[38] With these models, both the topology of the pore space and the pore shape (morphology) can be included.[34] They are, therefore, more representative of the pore space than the earlier models, and can be used to model complex mass transfer and reaction processes in porous catalyst particles, like multiphase reactions and catalyst deactivation by coking.[39] However, even such pore network models are still an approximation of the real void space in porous catalyst particles. With the recent advent of faster computers and powerful experimental instruments, it is becoming possible to digitally reconstruct a real porous catalyst particle with increasing accuracy. For example, X-ray microtomography and nanotomography can generate three-dimensional (3D) images of porous media without destroying the samples.[40] The digitally reconstructed pore models are more accurate in simulating mass transfer and reaction in a porous catalyst particle, but at the

cost of computational efficiency, and, even here, the resolution is limited in practice and reconstruction is typically based on small samples. Statistical methods that match various geometrical characteristics (surface area, pore volume, pore size distribution, etc.) with real samples can help to further improve the representation of a porous material. Digitally reconstructed models for a porous material can be reduced to pore network models, as a good compromise between accuracy and efficiency. Network extraction algorithms that may be used to achieve this include the thinning algorithm,[41] the medial axis based algorithm,[42] and the maximal ball algorithm.[43]

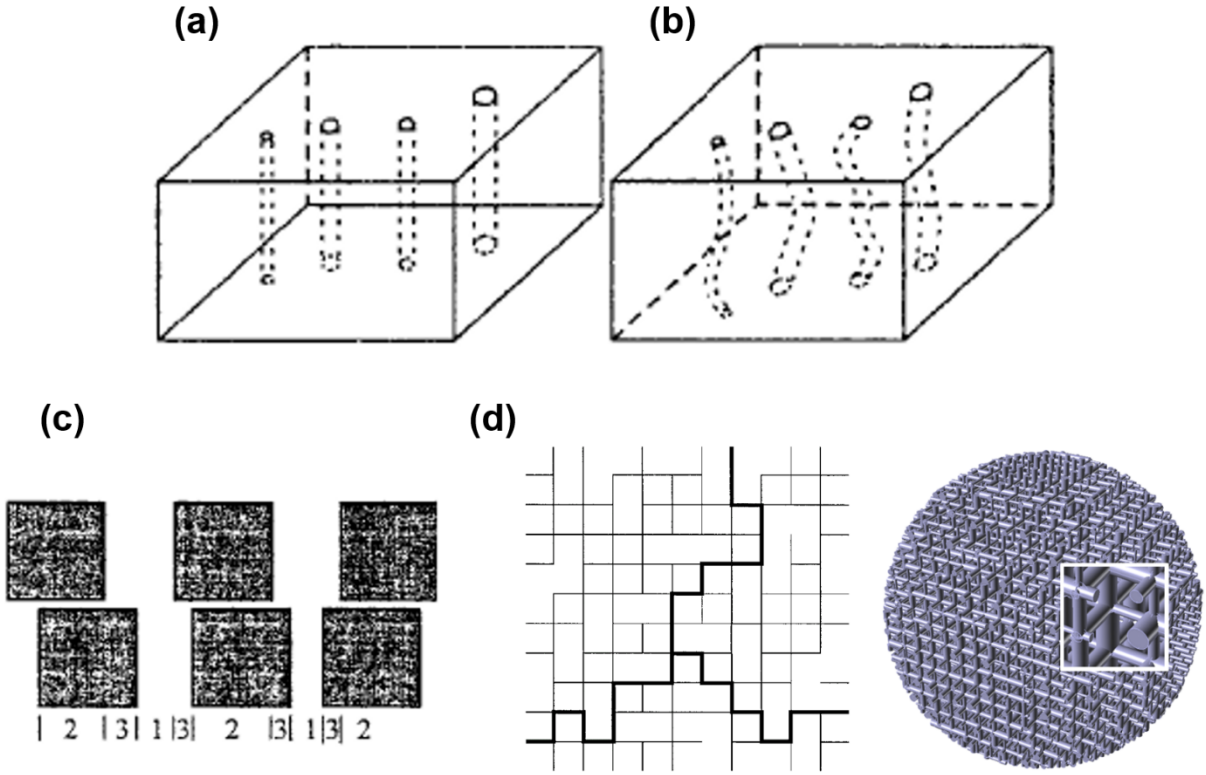

Figure 8. (a) Parallel pore model,[16a] (b) tortuous pore model,[35] (c) Model of Wakao and Smith,[36] and (d) pore network model.[22a, 38] Reprinted with permission from reference 16a. Copyright 1999 Elsevier. Reprinted with permission from reference 22a. Copyright 1999 Elsevier.

The structure of the pores and the pore network strongly influence the diffusion process in a porous catalyst particle, therefore, describing these influences is essential. Pore size and shape affect the diffusivity through molecule-wall interactions. Tortuosity is often used as a

structural parameter that characterizes the tortuous diffusion path in a porous catalyst particle, and can be defined as:

$$\tau = \varepsilon \frac{D}{D_{eff}} \quad (19),$$

where D and D_{eff} are the intrinsic and effective diffusivities. The tortuosity lumps many factors. It is significantly affected by geometrical parameters, but it could even be influenced by physicochemical factors, including the reaction rate.[16b, 44] Tortuosity tends to be higher when the pore size distribution is wider, the pore network is more heterogeneous, and the connectivity is lower. According to Eq. (19), a higher tortuosity corresponds to a lower effective diffusivity. For example, Hollewand and Gladden[45] reported a tortuosity of 138 for an artificially constructed pore network with a connectivity of 3 and spatially randomly distributed pores of two pore sizes differing by a factor of 10. However, tortuosities are not typically expected to be as high as this, as such pore networks of widely differing pore sizes tend to be hierarchical, with wider pores (e.g., macropores) surrounding particles with narrower pores (e.g., mesopores), as in Figure 7.

In addition, in amorphous porous catalysts or catalyst components, the pore walls are usually not smooth, but rough, and this surface roughness can also affect the diffusion process. The effect of surface roughness on the Knudsen diffusivity, D_K, can be approximated by:

$$D_K = D_{K0} \delta'^{D_f - 2} \quad (20),$$

where D_{K0} is the Knudsen diffusivity when the pore wall is smooth; δ' is the molecular diameter, normalized by the maximum of the fractal scaling range in the pore (often on the order of the pore diameter); and D_f is the fractal dimension of the walls, where $D_f = 2$ correspond to a smooth surface, $D_f = 3$ to a space filling surface, and $2 \le D_f \le 3$ for a general, self-similar surface (as is the case for many common amorphous supports, like silica

gel or γ-alumina). More details about the effect of surface roughness on diffusion and reaction in porous catalysts can be found in the literature.[46]

3 Nature-inspired optimization of hierarchical catalysts

3.1 Nature-inspired solution methodology

Studying natural transport networks can provide guidance to determine the optimal structure of the catalyst pore space. As discussed in the Introduction, scalable transport networks abound in nature, given the requirement to bridge the nano- and the macroscale, irrespective of the growth of the organ or organism. A tree grows through photosynthesis, mediated by a series of chlorophyll and metal oxide containing complexes with an intricate, hybrid structure that splits water, expels oxygen, channels electrons through a "Z-scheme", and provides the components (ATP and NADPH) to power the Calvin cycle that reduces carbon dioxide from the air into sugars, which polymerize into biomass. However, these processes at the nanoscale cannot occur without access to air and sunlight, as well as water, collected with nutrients from the soil, through a fractal root network, up the stem and through the tree crown to the leaves, where the active sites for photosynthesis reside. There is much to learn from photosynthesis at the nanoscale (including the geometrical, chemical and electronic structure of the components involved in the process), to develop bio-inspired catalysts for water splitting and CO_2 reduction, in search for solutions for renewable energy and sustainability.[47] Here, we are concerned with the arguably equally important processes at the meso- to macroscale: the leaves and the tree crown, without which such tree won't exist.

This is where the physics of transport phenomena come into play. Similar to the upscaling of chemistry in a test tube to a chemical reactor for production, efficient, scalable transport of molecules to and from the active sites is quintessential. The active sites, where reactions occur, need to be accessible via a molecular transport network; the veins of a leaf are replaced by the pores in a porous catalyst, which includes a high specific surface area, to increase the

overall production. There are clear parallels between the functional requirements of a tree, shown in Figure 9, and a catalytic reactor, depicted in Figure 3.

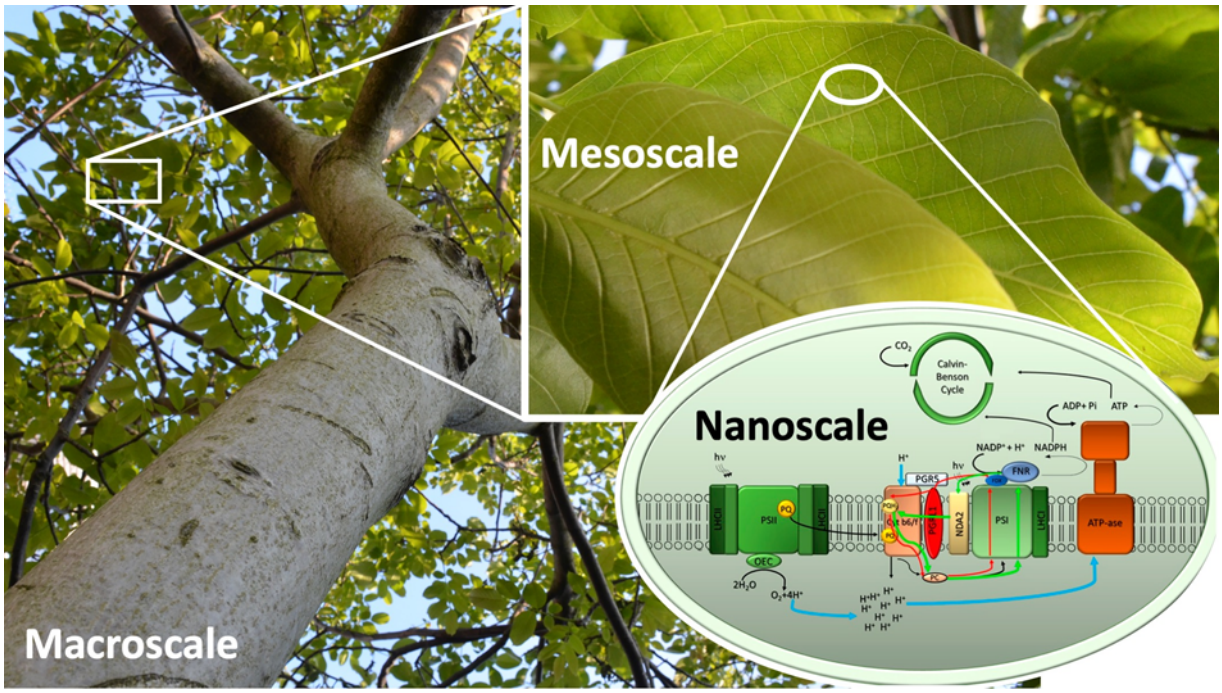

Figure 9: A tree as a bioreactor. All scales matter, from the photosynthetic complex (nanoscale), to the veins in the leave (mesoscale), and the fractal architecture of the tree crown (macroscale). There is a clear functional similarity with, respectively, the active sites, the catalyst pore network, and the catalytic reactor. Macro- and mesoscale photographs © M.-O. Coppens, nanoscale image from Vecchi et al.[48]

Remarkably, the specifics at the nanoscale might strongly differ, to serve different reactions or molecular transfers, but biological transport networks at larger scales share many structural similarities. For example, vascular and respiratory networks share the same features: fractal self-similar scaling at macroscopic scales (with gradually narrowing channels) transitions into a much more uniform distribution of channel sizes with interconnections between channels at the mesoscale.

Rather than taking these structural observations in nature as dogma in a narrow “biomimetic” approach, it is essential to understand the basis for this transition. After all, structural features in nature must typically address multiple objectives simultaneously (e.g., also mechanical

strength and access to sunlight for a tree). In addition, there should be no *a priori* assumption that nature must be optimal, let alone optimal for *our* purposes: the constraints in nature differ from those in industrial catalysis or other applications. An efficient use of resources is an essential constraint, only in as far as those resources are limited. For example, plants rarely exceed solar storage efficiencies of 1%.[47b] In nature, bottom-up synthesis and self-organization are powerful mechanisms, but they are often assisted by genetic instructions and subtle environmental cues, which are not easy to emulate. Some synthetic tools are more easily accessible by nature, while other, top-down manufacturing approaches and techniques that harness non-physiological conditions, such as higher temperatures and pressures, open up different opportunities in technology. Time scales are different and maximizing rates of reaction is rarely a goal in nature. Finally, economics, as well as the societal context and even the legal regulatory framework play a crucial role in industrial practice. In other words, the optimization space and the objectives themselves are often different in nature and technology – hence the need to exercise caution when "copying nature".[3b, 7, 49]

On the other hand, there are examples of scalability, efficiency, resilience and adaptability in nature that, by far, exceed those in technology, including in catalysis and reaction engineering. Therefore, a nature-inspired, rather than biomimetic approach starts with *scientific understanding* and consists of *extracting fundamental mechanisms that can be adopted, after proper adaptations, to an applied context*. This opens the door to innovation and ways to address specific limitations in a technical problem, where nature has evolved to achieve a superior, if not optimal solution for a similar problem.

This is the case for highly efficient, scalable transport networks. The universal features of such networks in nature stem from a need for the structures to scale, which is accomplished naturally through growth via self-similar branching, thus retaining function at the microscale, while simultaneously decoupling phenomena of macroscopic, global transport (via flow) and microscopic, local transport (typically, via diffusion) and reaction. One of the characteristics

of the nature-inspired solution approach is to note such *universal* features – in this case, the remarkable commonalities of hierarchical transport networks in nature – and to seek whether these may infer desirable properties.

At macroscopic scales, inspiration from the fractal architecture of trees and lungs has served to propose fractal distributors for chromatographic columns,[50] fluid injectors for fluidized beds[2, 51] and other multiphase reactors, and flow plates for fuel cells.[52] The fractal dimension, the branching ratios and the successive channel diameters are parameters that can be optimized, just like they are different in trees, lungs or the vascular network. In addition to being scalable and space-filling, the lung is thermodynamically particularly efficient[53], thanks to an optimized channel length and diameter scaling from one branching generation to the next (the cube of the diameter of the parent being the sum of the cubes of the diameters of the daughters, so-called Murray's law).[54] This specific scaling law allows us to breathe while consuming minimal metabolic energy, preserving energy for locomotion and the brain. Thus, the lung can teach us ways to distribute fluid with minimum thermodynamic losses (minimum entropy production) by using a similar, Murray's law-based sequence of channel diameters in a fluid distributor.

The transition from a fractal macro- to a uniform mesoscopic architecture turns out to coincide with the transition from flow to diffusion, corresponding to a Péclet number, $Pe \sim 1$.[3a, 52] Rather than copying the size of twigs or bronchioles in catalyst and reactor design, or complete a geometrical cascade arbitrarily, nature teaches us that the optimal transition occurs at that channel diameter where $Pe \sim 1$, as discussed by Vogel.[55] Theoretical and computational studies can demonstrate this, and we shall return to this in Section 3.2. For narrower diameters, a uniform distribution of channel or pore sizes suffices. For wider channels, a fractal cascade is beneficial, and not only for reasons of scalability, but to optimize the overall distribution and minimize entropic losses. This crossover depends on *Pe*: thus, it is not a fixed diameter that should be naively copied from a lung or a tree.

Using physical principles rather than superficial similarity (in geometry, size or perceived cause) is an essential difference between straightforward biomimetic and fundamentally grounded, nature-inspired engineering design. There is no reason at all to believe that the biomimetic approach will lead to better solutions, just because it mimics nature. Nature-inspired engineering is non-dogmatic and seeks guidance from nature on the basis of universal mechanisms. Apart from the principles underpinning the structure of hierarchical transport networks, discussed here, other ubiquitous mechanisms include: force balancing and nano-confinement effects (balancing mechanical forces at larger scales; steric constraints, electrostatics and polarization at the nanoscale), dynamic self-organization (associated to pattern formation and self-healing), and dynamic interaction networks in ecosystems[56] (associated to resilience and adaptability). All these can be used to develop nature-inspired designs for a wide range of applications, from biomaterials[49] to electrochemical devices[47e, 52] and dynamically structured fluidized beds.[51, 57] Here, we focus on hierarchical transport networks at the mesoscale, where similar structural features to those seen in leaves and tissues are found by computational optimization of this network in porous catalysts.

3.2 Computational optimization of hierarchical pore networks

The previous discussion demonstrates that rational design of porous catalysts should involve both the catalytically active sites and the pore network. The geometric and electronic structures of the active sites determine the intrinsic kinetics, while the pore network structure affects the observed reaction rates, which determine the overall yields and product selectivity in a catalyst pellet, and, ultimately, at the reactor outlet. The concepts introduced in Section 2 can help us optimize the catalyst pore network architecture, guided by the overarching, nature-inspired design principles of Section 3.1.

A leaf functions as a porous catalyst support, in which carbon dioxide and water are converted into sugar and oxygen. Thus, fast transport of these reactants and products are critical to the

success of this biochemical reaction system.[58] Leaves of many plants have developed a hierarchical channel system for transport, which can provide inspiration to design the pore networks of porous catalysts. The transition from fractal branching crown to more uniform veins in leaves is apparent in many trees; nevertheless, this does not tell us what the optimal leaf venation is – or what the optimal pore network properties in heterogeneous catalysis are, unencumbered by other complex constraints that leaves face, and which could influence leaf venation as well.[58]

In zeolite catalysts, a hierarchical pore network can be generated by introducing macro- and mesopores as "highways" for fast diffusion. However, these "highways" should be optimized to achieve a porous catalyst particle with high performance. The structural parameters for optimization should at least include porosity, pore size distribution, and zeolite crystal size, but could also include pore network connectivity and spatial crystal or porosity distribution. Recalling the various modeling approaches introduced in Section 2.3, more or fewer of these parameters can be included in the simulations, depending on the sophistication of the model. Such models can serve synthesis efforts in two ways: (1) investigate if *general* statements could be made, potentially with rules of thumb about the characteristics of the optimal hierarchical pore space, and (2) provide a modelling and optimization framework for *specific* catalytic reactions.

In a hierarchically structured catalyst particle, the mass transport of molecules can be divided into two diffusion processes: diffusion in the wide pores covering the whole catalyst particle, and local diffusion in the nanoporous "islands" surrounded by wide pores. The diffusion path through the network of wide pores is usually several orders of magnitude longer than that in the nanoporous "islands". Therefore, the rate determining process for mass transfer could also be in the wide pore network, even though the diffusivity in the wide pores is much larger than the one in narrow pores, such as the zeolite micropores. For example, Kortunov et al.[59] employed PFG NMR to experimentally study the mass transfer in composite faujasite zeolite-

containing particles used in fluidized bed catalytic cracking (FCC), and indeed found that the mass transfer at the reaction temperature is governed by diffusion in intercrystalline wide pores, rather than in the intracrystalline micropores, as is usually assumed (Figure 10). Thus, diffusion resistance in wide and narrow pores should both be considered when optimizing a hierarchically structured catalyst particle.

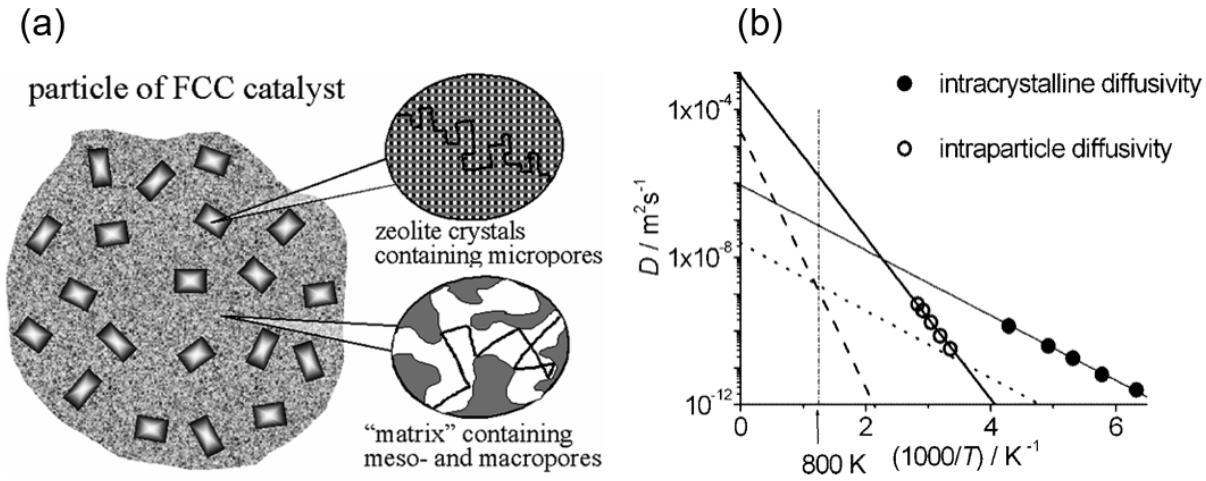

Figure 10. (a) Schematic illustration of a typical FCC catalyst particle; (b) the intraparticle diffusivity of *n*-octane in a FCC catalyst particle and the intracrystalline diffusivity of *n*-octane in large crystals of USY zeolite, measured by PFG NMR.[59] Reprinted with permission from reference 59. Copyright 2005 American Chemical Society.

Given their industrial importance, diffusion and reaction in hierarchical, bidisperse catalysts has been studied for many years, including by Wakao and Smith,[36a] Dogu[60] and Loewenberg,[61] who all indicated the importance of both micro- and macropores on the overall effectiveness factor. Gheorghiu and Coppens[62] developed a two-dimensional model to optimize hierarchically structured catalyst particles with a wide-pore network introduced into a nanoporous catalytic material for catalyzing a first-order, isothermal reaction (A→B). The size of the hierarchical catalyst particle or pellet is kept constant, as it often would be in practical applications. They found that a fractal-like network of wide pores is close to the optimal one that yields a maximized effectiveness factor. However, in this optimization, a constant number of wide pores was assumed, and this optimization does not guarantee that the apparent, observed reaction rate is maximized (viz. Eq. 2); after all, the total amount of

nanoporous catalytic material contained within a particle changes in this optimization. Wang et al.[63] relaxed the above constraint and compared monodisperse, bidisperse, and bimodal pore networks in a nanoporous catalyst for a first-order, isothermal reaction (Figure 11). A continuum model was used to solve the diffusion and reaction equations in each of the squares in Figure 11. Here, bidisperse means that the pore size in the wide-pore network is constant, unlike a bimodal pore network, where the size of the wide pores can vary at will. They found that the yield using an optimized bidisperse catalyst could be an order of magnitude higher than that using the original monodisperse, purely nanoporous catalyst, by significantly reducing the overall diffusion limitations. Remarkably, further optimizing the statistical and spatial distributions of pore size and porosity of wide pores does not appreciably increase the yield. Furthermore, Wang et al.[63] found that the distribution of the wide pore size is of secondary importance in determining the apparent activity of a catalyst particle, when compared to the total porosity associated to these wide pores, as long as the pores are sufficiently wide for molecular diffusion to prevail (Figure 11).

Therefore, as a rule of thumb, a spatially uniform wide pore network with uniform pore size is sufficient: bidisperse and bimodal pore size distributions result in almost the same maximum, observed reaction rate for a catalyst particle of a given size. It is most important to optimize the porosity and the average meso/macropore diameter, while the distribution around it is of secondary importance. A similar conclusion was also drawn when optimizing the hierarchical pore structure of zeolite adsorbents.[64] This is so, if the number of wide pores is large enough; otherwise, a fractal-like, wide pore network may lead to higher yield and effectiveness factor, demonstrating the importance of the optimization constraints.

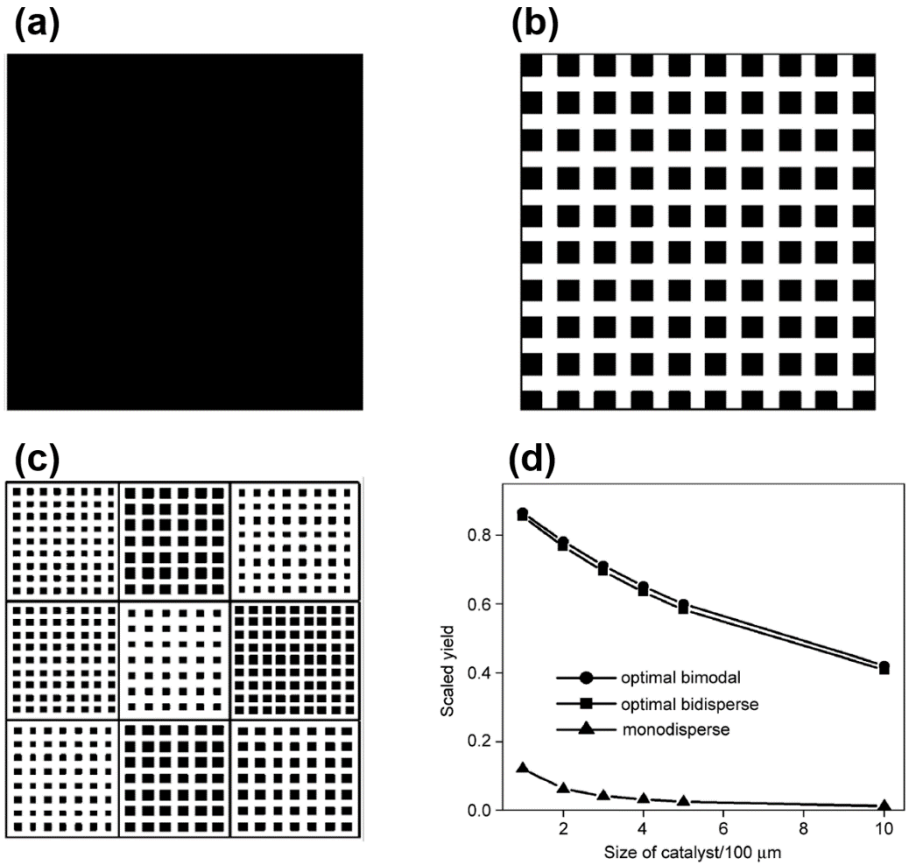

Figure 11. (a) Monodisperse structure that has a pore network with only narrow pores (e.g., pure zeolite); (b) bidisperse structure that has a hierarchical pore network, with narrow nanopores only in the black "islands" of the same size (e.g., constantly sized zeolite crystals) and wide pores of the same size surrounding these "islands"; (c) bimodal structure that is an assembly of $N \times N$ bidisperse substructures (in the illustration, $N = 3$), i.e., the zeolite crystal size is allowed to vary in $N \times N$ different zones of a pellet; (d) comparison of scaled yields of the monodisperse, optimal bidisperse and bimodal structures as a function of catalyst particle size (results shown for first-order reaction with $k = 100\ s^{-1}$, molecular diffusivity $D = 10^{-5}$ m^2/s, $D_{eff} = 10^{-9}$ m^2/s in the zeolite, mean free path is 100 nm).[63] Reprinted with permission from reference 63. Copyright 2007 Elsevier.

Introducing a wide pore network enhances diffusion, while it also reduces the amount of catalytic material in a catalyst particle. This indicates an optimal macroporosity when maximizing the apparent activity. Johannessen et al.[65] optimized the macroporosity of a periodic bimodal porous catalyst (see Figure 12), assuming pure molecular diffusion in wide pores and a first-order, isothermal reaction on the catalyst surface. For this model catalyst, the macroporosity (ε_{macro}) can be determined by:

$$\varepsilon_{macro} = \frac{d}{d+w} \qquad (21),$$

where *d* is the diameter of the wide pores and *w* is the pore wall thickness or the distance between the wide pores, occupied by nanoporous material, as illustrated in Figure 12. Here, it should be understood that ε_{macro} could stand for the porosity of wide mesopores as well: it is the porosity associated to the "highway network". It was shown that the optimal macroporosity is always at most 0.5. When *d* and *w* are optimized, concentration gradients in the nanoporous catalysts become indistinguishable, which is consistent with the results obtained by Wang et al.[63] Using optimal control theory, Johannessen et al.[65] also demonstrated more generally that allowing the pores to have a position-dependent diameter barely changes the optimum; hence, an optimized constant wide pore diameter, *d*, suffices. Also, the catalyst geometry (say, having a spherical pellet with a core-shell structure) has negligible influence on this general result, although it could save catalytic material to identify the shell in which most of the reaction in the optimized catalyst occurs and not introduce catalytically active material in the inactive core.

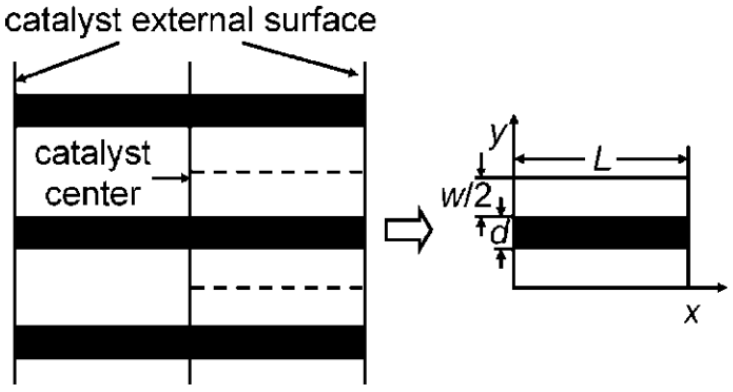

Figure 12. Schematic illustration of a bimodal catalyst slab (left) and of one of its subunits (right), used in modeling studies. The white parts are nanoporous catalytic material (e.g., zeolite); the black parts are wide pores.[65] Reprinted with permission from reference 65. Copyright 2008 American Chemical Society.

Real heterogeneously catalyzed reactions cannot often be approximated by a first-order reaction, yet Wang and Coppens[66] showed that the above results hold even more generally, for arbitrary reaction kinetics, $r = r(C)$. They proposed a general procedure to determine the

optimal porosity, ε_{opt}, w_{opt} (and, thus, pore diameter, d_{opt} from ε_{opt} and w_{opt} via expressions like Eq. (21)), and corresponding maximum yield and effectiveness factor, η_{opt}, for a hierarchically structured, nanoporous catalyst, such as a zeolite. For the detailed derivation, we refer to the original article, but the procedure goes as follows.

A generalized, *modified* Thiele modulus is defined, similar to Eq. (4) for a first-order reaction:

$$\phi_0 = w\sqrt{\frac{k}{D_m}} \tag{22}$$

or Eq. (7) for general kinetics:

$$\Phi_0 = \frac{V}{A}\frac{r(C_0)}{\sqrt{2}}\left[\int_{C_c}^{C_0} D_m r(C)\,dC\right]^{-1/2} \tag{23}$$

but with D_{eff} substituted by D_m, because it is (molecular) diffusion in the wide pores that determines the optimum. For an optimized, hierarchically structured zeolite catalyst, there are no appreciable diffusion limitations within the zeolite crystals. Eq. (23) requires only the evaluation of an integral, which can be done analytically for simple kinetics. The equation contains only known parameters; the concentration at the center is assumed zero for strongly diffusion limited reactions.

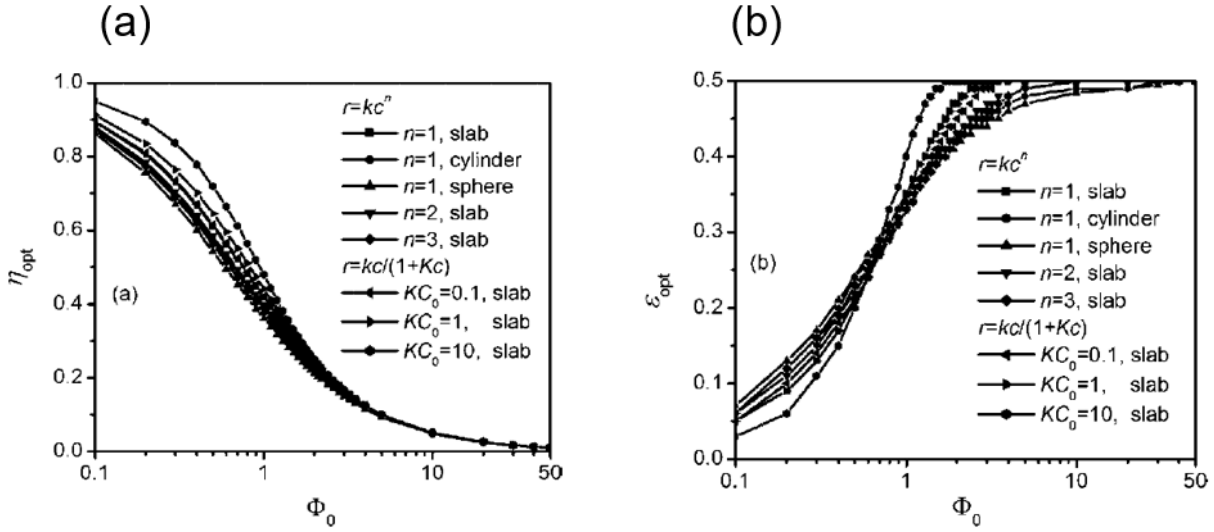

Figure 13. (a) Effectiveness factor and (b) macroporosity in the optimized hierarchically structured catalyst, for a range of kinetic expressions (first, second, third order and Langmuir-Hinshelwood kinetics for different adsorption constants, *K*) and different catalyst geometries.

The curves are very close, irrespective of kinetics or catalyst pellet shape.[66] Reprinted with permission from reference 65. Copyright 2008 American Chemical Society.

Following this, the optimal porosity and effectiveness factor can be read from Figure 13, which shows that the results are only weakly dependent on the details of the kinetics or the catalyst pellet shape. The maximum nanoporous catalyst (zeolite crystallite) size to avoid appreciable diffusion limitations within can be estimated from Eq. (22) or (23), but now using the (much smaller) diffusivity in the zeolite of the key component, D_z, instead of D_{eff}, and determining the length parameter, $w = \left(V / A\right)_z$, such that $\Phi_z \approx 1$. For example, for a quasi-spherical crystal particle and first-order kinetics, the crystal diameter would be $6\sqrt{D_z / k}$. This is the "rule of thumb" alluded to earlier: a quick estimate of the parameters determining the optimum hierarchically structured catalyst (ε_{opt} and w_{opt}), which provides the desired specifications for catalyst synthesis, no longer requires the explicit solution of any differential equations – only an integral and the use of a standard curve, $\eta_{opt} = \eta_{opt}(\Phi_0)$, which provides the effectiveness factor of the optimized pellet as well! For very strongly diffusion limited reactions, the optimal porosity, ε_{opt} = 0.5.

Using this methodology, Wang and Coppens[66] optimized a washcoat catalyst consisting of a mesoporous catalyst for the selective catalytic reduction of NO_x. They showed that the apparent activity of the catalyst (and its effectiveness factor) can be increased by a factor of 1.8-2.8 after introducing an optimal macroporosity $\varepsilon_{macro} = \varepsilon_{opt}$ = 0.2-0.4 for a washcoat thickness of 0.5-1.5 mm. In subsequent work, Wang and Coppens[67] also optimized a commercial, mesoporous Ni/Al_2O_3 catalyst for the autothermal reforming of methane. They found that the apparent activity can be increased by a factor of 1.4-4 by only adjusting macroporosity and macropore size of the catalyst. In addition, they also demonstrated that the CO/H_2 ratio or the selectivity toward CO can be increased by reducing the macroporosity,

indicating that the pore network structure can be used as a handle to control the selectivity in the produced syngas. More recently, Liu et al.[68] introduced macropores into mesoporous Rh/Al_2O_3 catalyst pellets for dry reforming of methane. They showed that optimizing the macroporosity can lead to a 56-175% increase in apparent activity and a 10-18% reduction in the use of catalytic material.

The catalyst stability can also be affected by pore network structure and optimizing it can mitigate deactivation by fouling. Rao and Coppens[69] optimized a mesoporous hydrodemetalation catalyst. By introducing an optimal hierarchical pore network, they maximized the overall catalytic activity and robustness to deactivation over a given time on stream, from catalyst particle to fixed bed reactor level. This is schematically illustrated in Figure 14. The results show that the lifetime of this optimized hierarchically structured, meso/macroporous catalyst can be extended by 40%, while using 29% less catalyst than a non-optimized, purely mesoporous catalyst. Shi et al.[70] further optimized the hierarchically structured hydrodemetalation catalyst by considering the effect of the concentration profile in the reactor, and they found that its lifetime can be further extended. Earlier work by Keil and Rieckmann[71] found that pore connectivity also has a significant influence on the stability of a hydrodemetallation catalyst. A well-connected pore network is more robust against catalyst deactivation by fouling.

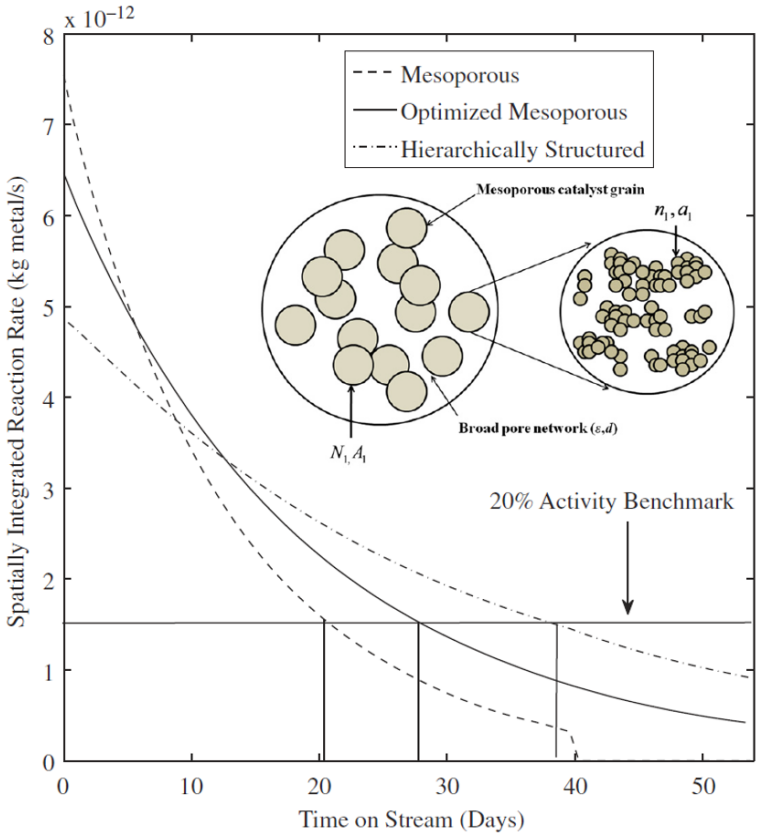

Figure 14. Comparison of the catalyst lifetimes of mesoporous, optimized mesoporous, and hierarchically structured hydrodemetalation catalyst particles. The insert illustrates the hierarchically structured catalyst.[69a] Reprinted with permission from reference 69a. Copyright 2012 Elsevier.

Fouling in a porous catalyst particle can plug pores and, sometimes, the fraction of plugged pores can reach the percolation threshold, where continuum models break down. Ye et al.[39a, 39b] developed a pore network model that is able to describe diffusion and reaction, accompanied by pore plugging, and they used this pore network model to optimize a Pt-Sn/Al_2O_3 catalyst particle for propane dehydrogenation (see Figure 15). They found that the optimized hierarchically structured catalyst particle can be 2.8 times more active and save 45% catalyst weight when compared to a mesoporous benchmark catalyst. Pore network models have also been developed to investigate the catalyst deactivation caused by phase change. Liu et al.[72] probed the short-term deactivation caused by sulfur condensation in alumina catalysts for the Claus reaction. They found that a Claus catalyst with a reasonable hierarchical structure is more robust against this short-term deactivation.

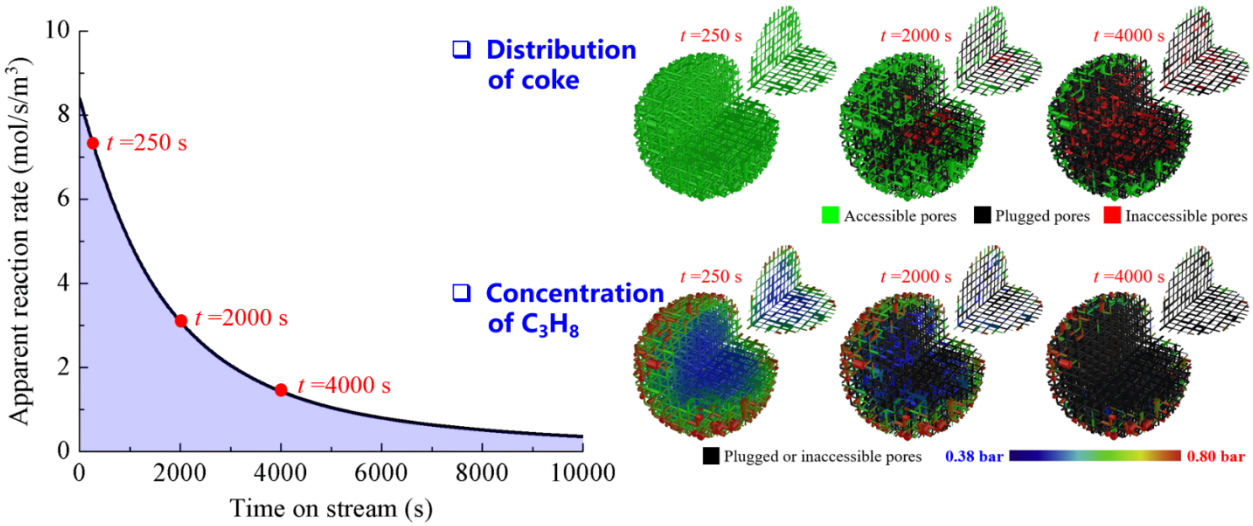

Figure 15. The catalyst deactivation by coking in Pt-Sn/Al_2O_3 catalyzed propane dehydrogenation, probed by a pore network model.[39a, 39b]

These previous examples all involved mesoporous catalysts, in which macropores were introduced. For microporous catalysts like zeolites, the same modeling approach could be used, however with notable differences at the level of the zeolite crystal, due to the different diffusion mechanism in the micropores. In zeolites, diffusion is dominated by intrinsically much slower configurational diffusion, due to strong molecule-wall interactions. In addition, it can be difficult to decouple the intrinsic reaction kinetics in micropores from the intracrystalline diffusion behavior; both are coupled activated processes operating in concert under strong confinement. Quantum-mechanical calculations can yield the rate coefficients for the elementary steps, and molecular simulations can provide diffusivities and adsorption isotherms within zeolite crystals. Quantum and statistical mechanical simulation approaches to elucidate transport in micropores have been extensively reviewed, and will not be discussed here in detail.[22, 73] Hansen et al.[74] developed a multiscale model to quantify diffusion and reaction in a H-ZSM-5 crystal for benzene alkylation with ethene. In their model, a multi-component, Maxwell-Stefan equation with diffusivities obtained from molecular simulations was used to describe diffusion, and microkinetics determined from quantum chemical calculations were employed to describe reaction. Vandegehuchte et al.[75] developed a similar

continuum model for the more complex case of *n*-hexane hydroisomerization in a Pt/H-ZSM5 catalyst. Li et al.[76] included the diffusion in meso-/macropores in the continuum model for H-ZSM-5 catalyzed benzene alkylation with ethene, and they found that a catalyst with 62.3% of its volume occupied by randomly distributed H-ZSM-5 crystals maximizes the effectiveness factor. Ding et al.[77] developed a pore network model that also includes diffusion in meso-/macropores, and they concluded that intercrystalline pores and the crystallite orientation in a ZSM-5 membrane catalyst for xylene isomerization can significantly affect its catalytic performance. However, these aforementioned models for zeolite catalysts did not consider the effects of surface barriers on molecular transport. Rao et al.[6a] included external surface diffusion barriers in a multiscale, continuum model for H-ZSM-5 catalyzed benzene alkylation with ethene, using the multiscale representation of the zeolite composite depicted in Figure 7, and employing first-principle calculations at the level of the individual zeolite crystals, similar to Hansen et al.[74] They found that the zeolite surface diffusion barriers cannot be neglected, otherwise the model cannot predict the experiments even qualitatively. This means that these barriers should be included in modeling and optimization studies. Due to their microporous structure, zeolite catalysts are prone to deactivation by fouling. Cai et al.[78] built a discrete model using graph theory and small-world networks, which is able to bridge the gap between microscopic physics and macroscopic catalyst engineering. Gao et al.[79] developed a deep data method by coupling multiscale reaction-diffusion simulations and super-resolution structured illumination microscopy to explore the characteristics of the SAPO-34 catalyzed methanol-to-olefins reactions. This method realizes the direct visualization of the spatiotemporal evolution of molecules (including coke) and active sites in a micrometer-sized crystal, while conventional imaging techniques can only provide limited information with probe molecules or catalysts of large size.

These studies show that a well-designed hierarchical pore network in a catalyst particle or pellet can increase catalytic activity, selectivity and stability remarkably, without changing the structure at the nanoscale, in particular the active sites themselves. Within the context of NICE, this hierarchical pore network is structurally similar to those found in nature, such as the uniform distribution of transport channels in leaves and tissues, when diffusion is the dominant transport mechanism. Performance is maximized for (1) a uniform distribution of the channels, with (2) a constant size of the zeolite crystals, similar to the cell size in biology. Most important, and useful as a practical tool to guide synthesis efforts, are the optimal porosity and the cell/crystal size, as well as to have sufficiently wide pores in between to avoid undesired additional diffusion limitations within individual crystals that would affect the intrinsic product distributions. Such a hierarchical structure also facilitates scalability, both in nature and in chemical reactor engineering, for example by using the fractal distribution networks discussed earlier, which have been implemented in fuel cells and fluidized beds.

An interesting question, as yet unanswered, is how these surface barriers come into play and whether, also here, lessons could be learnt from nature? Certainly, membranes are nature's most common interface for exchange and molecular separation, including in and around cells, within which reactions occur. Since the studies of Rao et al.[6a] and Guo et al.[6b] point out the key role of, respectively, external and internal surface barriers in optimizing catalyst performance for some zeolite catalyzed processes, we conjecture that the optimization of hierarchically structured zeolites could benefit from a closer look at how to translate the mechanisms of biological membranes, which function as interfaces, to design more intensified catalytic processes, which integrate catalysis, transport and separation.

4. Synthesis of hierarchically structured zeolites

The previous section discussed how to optimize hierarchical pore systems in order to design catalysts with better mass transport properties. The transport pore system must exhibit an optimal porosity, consisting of wide enough meso- or macropores, and the zeolitic domains between the transport pores need to be small enough to eliminate local diffusion limitations. Over the last years, great progress has been made in synthesizing hierarchically structured zeolitic materials, which should help to realize structures guided by the computational optimization results. Nevertheless, control over all aspects of the generated additional pore network, for a particular catalytic system, remains a challenge.[80] Many techniques focus on one aspect of the additional pore system, but to design an optimal hierarchical zeolite, all aspects of the hierarchical pore system, as well as the zeolite material characteristics, such as the strength and distribution of its acid sites, need to be considered.

The synthesis of a hierarchical zeolite catalyst should allow effective control over the following characteristics:

- (1) *Pore size distribution*: The pore size of the additional transport pores determines which diffusion mechanism is dominant. Its size can change catalytic performance, including catalyst lifetime.[81] While it was shown earlier that it is the average size of the wide pores that matters most, this pore size tends to be in the macropore range, in particular for gas phase reactions, to avoid Knudsen diffusion to become limiting, rather than molecular, bulk diffusion. Many synthesis efforts on including tailored pore sizes and distributions in zeolites have focused on the introduction of mesopores, and there are far fewer works on introducing macropores in a well-controlled manner[82],[83],[81].
- (2) *Pore volume*: The additional porosity, affecting the total pore volume and total porosity, is another important characteristic of hierarchical zeolites. In case of constant pore size, a higher porosity results in a larger surface area and reduced

diffusion path lengths within the microporous domains. Experimentally, increased catalytic performance could indeed be observed with increasing pore volume. For example, increased mesoporosity led to higher conversion in pinene isomerization or a prolonged catalyst lifetime in the methanol-to-olefins (MTO) process.[84]

- (3) *Pore connectivity*: The mass transport properties of a hierarchical zeolite depend on the connectivity of the additional, wide pores to the micropores and in between each other. As shown by de Jong and co-workers, using electron tomography, isolated pores may occur in zeolite Y, used in catalytic cracking, which do not effectively enhance mass transport and, thus, are much less beneficial for the overall catalytic performance.[85] Another good example of this effect is the reduced catalytic performance of zeolites with constricted mesopores compared to connected mesopores, as reported by Milina et al.[86] However, unless severe constrictions due to rapid catalyst deactivation occur (as is the case in catalytic cracking), the impact on overall yields and selectivity may not be significant, as long as well-connected paths are present that traverse both the zeolitic and the meso/macroporous domains.
- (4) *Zeolite material characteristics*: Besides the mentioned characteristics of the additional pore system, the microstructural catalytic characteristics, such as chemical composition, crystallinity, and acidity or basicity need to be maintained at their optimal values. This can often be challenging, due to the major alterations resulting from synthesis or post-synthetic procedures, which are used to generate the hierarchical pore system. More generally, the independent control over all textural parameters and the intrinsic zeolite crystal characteristics is not trivial. *A good-looking hierarchical structure does not imply a better catalyst*!

This section will discuss selected synthesis routes for hierarchical zeolites, focusing on how effective they are in controlling the different properties of the generated additional pore

system. We do not intend to be exhaustive in our review, but rather illustrative, and highlight a few pathways to realize the designs discussed in the previous sections, focusing mostly on synthesis routes for all-zeolite materials. This does not mean that composites, such as the structure shown in Figure 7, are unimportant. On the contrary, they are an extremely useful way to realize hierarchical catalyst structures, as exemplified by FCC catalysts, which combine intra- and intercrystalline pores.

The commonly used synthesis routes for hierarchical zeolites can be divided into bottom-up techniques, which generate a hierarchical pore system during the zeolite synthesis, and top-down approaches, which post-synthetically generate an additional pore system in parent zeolites.

4.1 Bottom-up approaches

4.1.1 Hard-templating methods

Additional solid particles that are present during the synthesis of zeolite crystals can template the generation of intra- or intercrystalline pores, a process called "nanocasting".[87] This technique allows to generate additional porosity, ranging from small mesopores to macropores. Examples of commonly used hard templates include polystyrene spheres,[82] carbon materials (carbon black,[88] carbon fibres,[89] carbon nano tubes[90]), mesoporous silica particles[83] and resins.[91] The added particles act as sacrificial templates, which are typically removed by combustion during calcination.

The resulting pore sizes can be controlled very effectively by changing the particle size of the used hard template.[81] Furthermore, by changing the amount of hard template added to the synthesis mixture, the pore volume of the additional porosity can be adjusted. However, while the hard-templating method allows for great control over pore size and pore volume, the control over the pore connectivity is challenging. Especially if the fraction of hard template is reduced to lower the pore volume, isolated pores can be generated.

One attractive aspect of this method is the possibility to generate macropores of a controlled size, which are not easily obtainable using any other methods. Computational optimization of hierarchical pore systems has shown that the optimal pore size for selected reactions is often in the macroporous range (> 50 nm).[66] Therefore, the hard-templating method might be at an advantage in terms of obtainable pore sizes. One drawback of the method is the template removal, which could damage the zeolite framework. However, recent work by Machoke et al. used mesoporous silica particles as a sacrificial template, which acts as silicon source during crystallization, thus allowing to eliminate the template removal step.[92]

4.1.2 Soft-templating methods

This bottom-up approach uses supramolecular arrangements of surfactant molecules, e.g., micelles, as a template for the formation of mesopores during zeolite synthesis. Three main types of soft templating techniques are commonly applied: Surfactant assisted assembly of zeolite nanocrystals[93] and the use of organosilane surfactants[94] or bi-functional surfactants with a zeolite structure-directing agent (SDA) for the generation of zeolite nano-sheets.[95]
The formation of nano-sheets by using bifunctional surfactants was discovered by Ryoo and co-workers.[96] The specially designed surfactants consist of a long, hydrophobic alkyl chain and hydrophilic quaternary ammonium head groups. The quaternary ammonium head groups act as the structure-directing agent for the formation of the MFI zeolite, and the hydrophobic interaction between the surfactant chains causes the formation of a micellar structure. Recent work demonstrated that, first, a layered silicate is formed, which, subsequently, transforms into zeolite nanosheets during the crystallization process.[97]
The surfactant assembly can be controlled very well by, e.g., changing the surfactant chain length or the functional groups or by altering the packing parameters via the addition of swelling agents.[98] This allows for good control over the resulting pore size and mesoporosity. Additionally, macropores are often formed by the intergrowth of these zeolite

layers, giving rise to a trimodal pore size distribution. The dimensions of the interlayer mesopores are set by the used surfactant and are very well defined. However, the range of pore sizes generated is limited to mostly small mesopores. Control over the macropores is even more challenging and depends on synthesis parameters, such as temperature and gel composition, but also post-synthetic treatments, such as calcination. Overcoming such limitations is important, given what was mentioned earlier about the need to create controllable macropores or wide mesopores to form transport "highways".

4.1.3 Non-templating methods

Methods that do not require a template are very appealing, due to the high cost and environmental concerns of using soft and hard templates. Current template-free, bottom-up methods are based on the aggregation of nanocrystals,[99] the crystallization of porous, amorphous gels[91] and the modification of the zeolite growth.[100]

Especially the modification of the zeolite growth to generate layered zeolites without the addition of organic templates represents a green and very promising alternative to the use of soft templates. The layer formation relies on the repetitive branching caused by the formation of small domains of a second isostructural zeolite (structural twin) within the zeolite framework, such as EMT domains in FAU zeolites or MEL domains in MFI zeolites. The assembly of the layers results in intercrystalline porosity. Initially, the formation of the structural twin was facilitated by the addition of salts, but recent publications demonstrated that it is also possible to synthesize layered zeolites additive-free by changing the synthesis temperature.[101] The generated additional porosity is not as well defined as the mesopores in samples prepared by using soft templates and the control over the mesopore size is also more challenging. However, it could be shown that changes in synthesis parameters, such as temperature and water content, allow a certain control of the additional porosity, as well as the crystal morphology.[102] Besides limitations in controlling the pore size, another drawback of

this technique is that it is only applicable to certain zeolite topologies that have an isostructural twin such as MFI/MEL and FAU/EMT.

Another appealing non-templating approach for the synthesis of mesoporous zeolites is to use the organic structure directing agent, necessary for the zeolite crystallization, also as a scaffolding or templating molecule for the mesopore formation. For this approach, two different synthesis methods have been reported in the literature.[103] Both synthesis methods are based on two-step procedures and are closely related. The first one uses hydrothermal crystallization to synthesize zeolite nanocrystals and forms the mesopores in a subsequent gelation step at room temperature.[104] The other technique starts with the formation of the mesostructured aluminosilicate by gelation, followed by dry gel conversion to crystallize the zeolite phase.[105] The mesoporous zeolites synthesized following these two techniques are called TUD-M and TUC-C, respectively. The synthesis without any additional templates, the relatively simple process and the good control over the mesopore size are advantages of this set of methods. However, even in the case of TUD-C, the hierarchical zeolite is not completely crystalline and thus represents a composite, consisting of zeolite crystals and amorphous silica/alumina phase, with potentially different Si/Al ratios.

Figure 16 shows examples of hierarchical zeolites synthesized using the bottom-up methods discussed in this section.

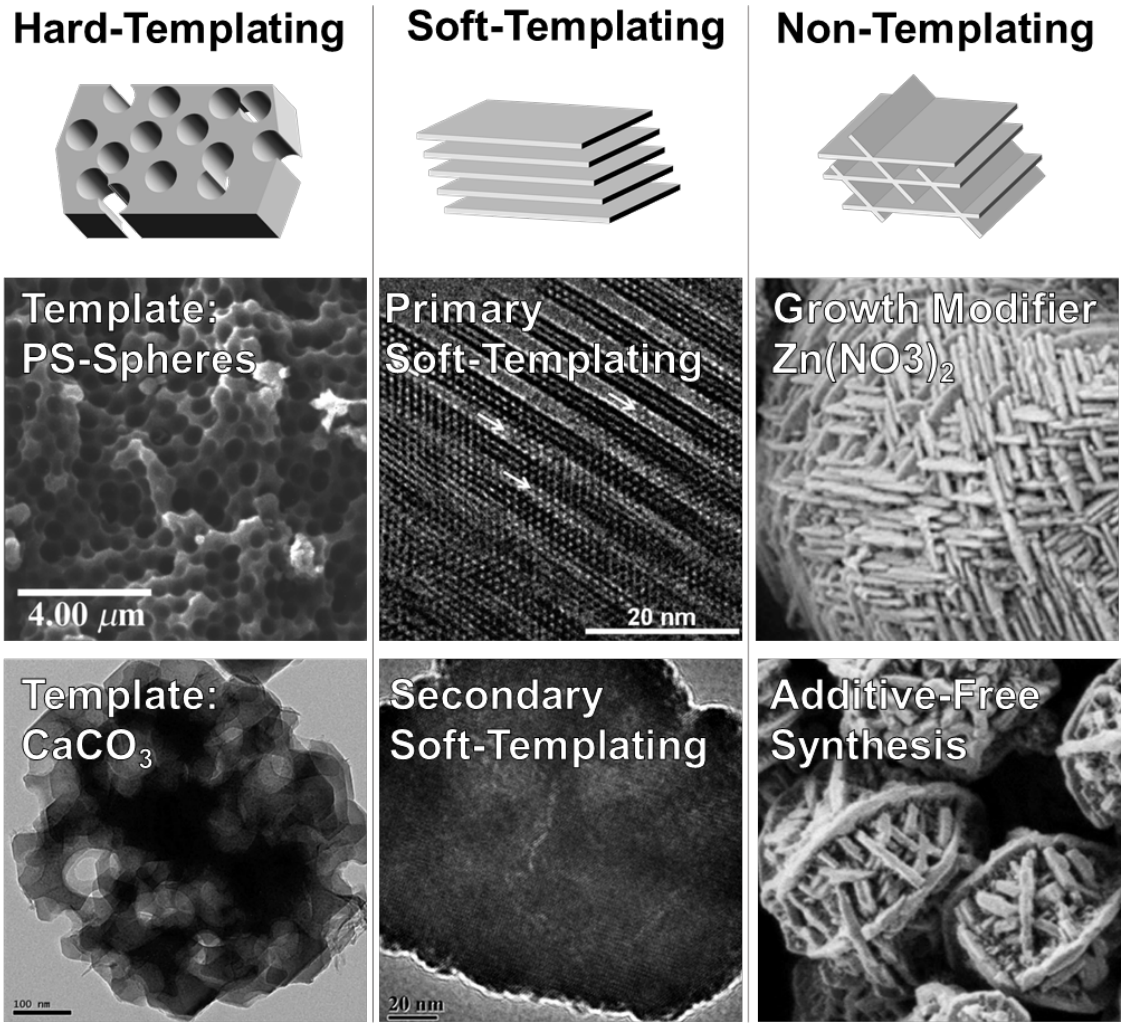

Figure 16: Schematic representation (top row) and electron microscope (SEM/TEM) images of examples of hierarchically structured zeolites, synthesized using bottom-up methods. Reprinted with permission from reference 82. Copyright 1999 American Chemical Society. Reprinted with permission from reference 93. Copyright 2011 Wiley-VCH. Reprinted with permission from reference 100. Copyright 2015 Royal Society of Chemistry. Reprinted with permission from reference 102. Copyright 2020 Springer Nature. Reprinted with permission from reference 106a. Copyright 2008 American Chemical Society. Reprinted with permission from reference 106b. Copyright 2010 American Chemical Society. [82, 93, 100, 102, 106]

4.2 Top-down approaches

4.2.1 Demetallation

Additional pores in zeolite crystals can be generated by partial removal of framework atoms, such as Si or Al, by steaming or leaching with acids or bases. Dealumination by steaming or acid treatment has been used for many years to reduce the Brønsted acidity of zeolite Y to generate USY zeolites used in FCC catalysts. The removal of Al also results in the formation of mesopores, but these pores are often poorly interconnected. The selective removal of Si, by

desilication treatment in alkaline solutions, is a more efficient way to create intracrystalline mesopores in zeolite crystals. The treatment has a much smaller impact on the acidic properties and crystallinity of the zeolite compared to dealumination and the generated pores are more interconnected. Verboekend et al. successfully established effective control over the generated pore system in terms of pore volume by correlating process parameters, such as alkalinity, treatment temperature and time to the properties of the obtained hierarchical zeolites for different types of zeolites and different Si/Al ratios.[107] Desilication by alkaline treatment is limited to aluminum-containing zeolites, with a Si/Al ratio of 25 in the parent zeolite being optimal for mesopore formation. Effective formation of mesopores by desilication of high silicon zeolites or even purely siliceous zeolites is possible by the addition of pore directing agents such as TPAOH (tetrapropyl ammonium hydroxide).[108] One drawback of the desilication method is the limited control over the pore size distribution, compared to the templating methods. Additionally, achieving connectivity of the additional mesopores can also be challenging.

The pore sizes that can be generated by demetallation are usually in the mesopore range. Only a few examples report the formation of larger macropores by using extensive desilication treatments.[109] However, the generated macropores are isolated voids within the crystal, resulting in hollow crystals. This restriction to small pore sizes represents a major drawback of the demetallation method.

4.2.2 Delamination and assembly

Delamination describes the treatment of layered zeolite precursors in alkaline media to expand the layers and intercalate surfactants. The intercalated zeolite layers are then separated by, e.g., sonication, followed by calcination of the sample to remove the surfactant. The resulting, randomly packed zeolite layers usually possess a high degree of interlamellar mesopores but can also partially condense and lose porosity.[110]

To avoid collapse and condensation of the layers and the consequent loss of mesopores, a pillaring step can be used to maintain the porosity after removal of the surfactant by calcination and, thus, increase control over the generated hierarchical porosity.[111] The pillaring step usually follows the intercalation of the layered precursor with surfactants. The surfactants, located in the interlamellar space, are impregnated with a silica source, such as a silicon alkoxide (e.g., tetraethyl orthosilicate, TEOS). The impregnated silicon alkoxide is then hydrolyzed to form silica, before the sample is calcined to remove the surfactants, and resulting in stable pillars that preserve the interlamellar mesoporosity.[106b]
However, even with pillaring, the control over both the resulting mesopore size and the total mesoporosity is limited.[111b] Furthermore, the delamination method is only applicable for certain zeolites that possess layered features, such as MWW, FER, SOD or MFI topologies.[110]

4.2.3 Mixed methods

4.2.3.1 Surfactant assisted meso-structuring

This top-down method combines dissolution under very mild conditions with soft-templating using surfactants. [112] Mesopores are generated in parent zeolite crystals by a one-pot treatment in a mildly alkaline, surfactant containing solution. The used soft templates are commercially available surfactants, such as cetyltrimethyl ammonium bromide (CTAB). During the meso-structuring, the alkaline environment facilitates the breaking of Si-O-Si bonds, forming negatively charged $Si\text{-}O^-$ groups. Because of electrostatic interactions between positively charged surfactants and negative defects, surfactants can enter voids in the zeolite and form micelles. The micelles then act as soft template during the rearrangement of the zeolite, giving rise to mesopores between 2.5 and 4 nm, depending on the chain length of the used surfactant. In contrast to desilication, the meso-structuring was reported to achieve the

post-synthetic formation of mesopores with lower zeolite loss and smaller decrease in crystallinity.

Mesoporous zeolite Y prepared following this method was tested as catalyst for the fluid catalytic cracking at a commercial scale and showed very promising hydrothermal stability, as well as selectivity.[113]

4.2.3.2 Dissolution recrystallization

The preparation of mostly mesoporous zeolites by this mixed method consists of a dissolution step, followed by a hydrothermal recrystallization step.[114] In the first step, the parent zeolite is partially dissolved by an alkaline treatment in the presence of surfactants, which prevent the complete dissolution by adsorbing to the zeolite surface. During this step, very small zeolite species are formed. In the following hydrothermal recrystallisation, the mixture is treated at elevated temperature and the small zeolite species recrystallize. In this step, the surfactant micelles act as mesoporogen, templating the formation of mesopores in the material. The prepared materials have zeolitic characteristics, but also some of the textural properties of mesoporous silica materials, such as MCM-41 (when CTAB is used as surfactant). Depending on the process conditions, different composites, such as zeolite coated mesoporous materials, but also hierarchically structured all-zeolite materials can be obtained.[115]

Figure 17 presents an overview of selected top-down synthesis methods of hierarchically structured zeolites.

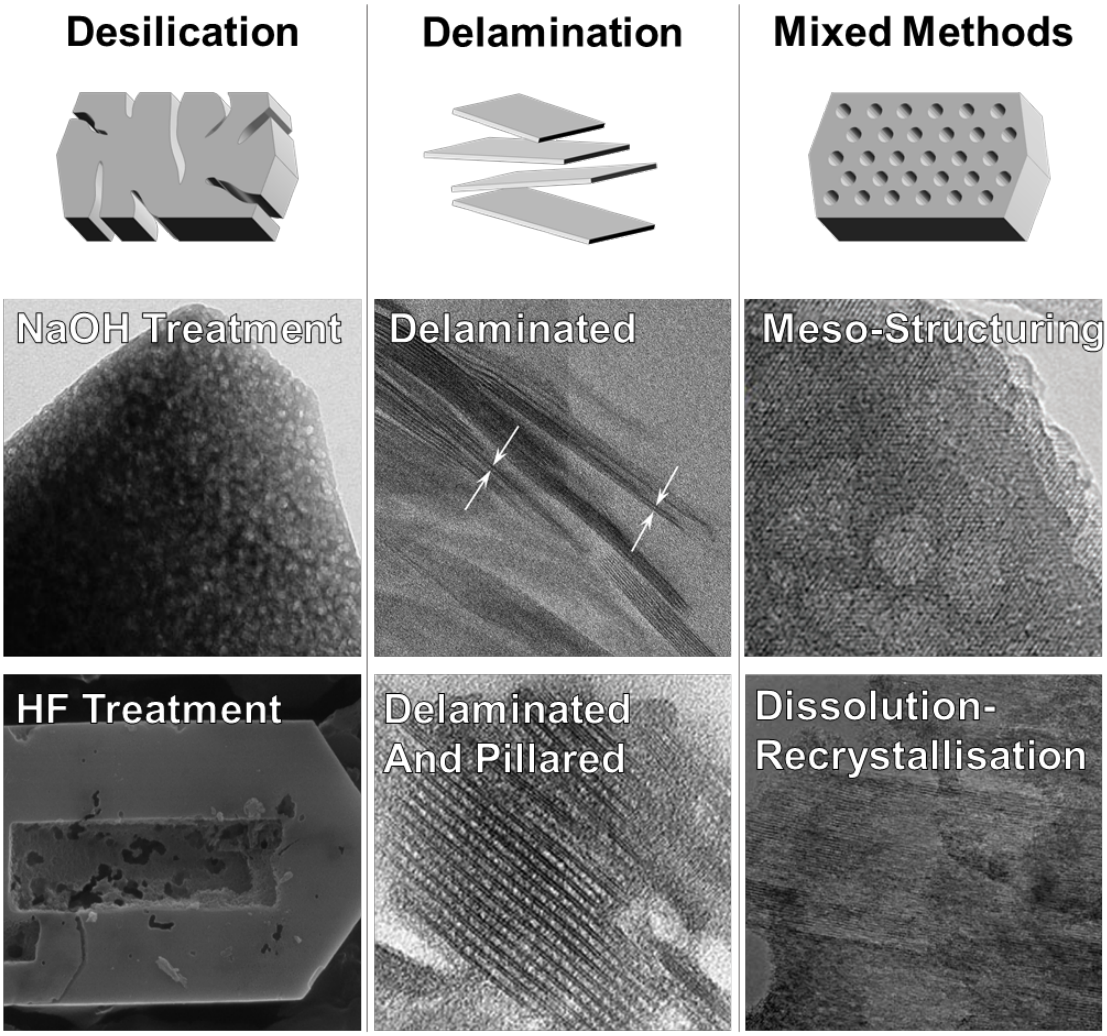

Figure 17: Schematic representation (top row) and electron microscopy (SEM/TEM) images of examples of hierarchically structured zeolites, synthesized using top-down methods. Reprinted with permission from reference 116a. Copyright 2011 Wiley-VCH. Reprinted with permission from reference 116b. Copyright 2013 American Chemical Society. Reprinted with permission from reference 116c. Copyright 2011 American Chemical Society. Reprinted with permission from reference 116d. Copyright 2008 American Chemical Society. Reprinted with permission from reference 116e. Copyright 2012 Royal Society of Chemistry. Reprinted with permission from reference 116f. Copyright 2004 Elsevier.[116]

4.3 Overview

In summary, the synthesis of hierarchically structured zeolites has evidently progressed a lot over the last years and, nowadays, allows for the synthesis of a multitude of different materials.[117] However, many methods only allow to generate pores with dimensions within a small range.[80b] While new ways to tune the additional pore system have emerged over the years, it is still not trivial to put computationally optimized designs into practice. Table 1 shows the limitations and advantages of different synthesis approaches for hierarchically

structured zeolites in terms of their ability to control the additional, macro- and mesoporosity. A further challenge is to translate some of these synthesis methods from the bench scale to the industrial scale, in particle or pellet formulations that are mechanically stable, and to do so in an economical and environmentally sound way.[118] Unfortunately, there is an opposite trend between the degree of tunability indicated in Table 1 and the economics; for example, hard-templating approaches offer us the most control, but they are particularly costly, while soft-templating and non-templating approaches offer less control, but the absence of expensive templates is an advantage. The distribution of Al in the material is clearly extremely important in catalysis and is one of the challenges when demetallation routes are used to control porosity at the same time.

Table 1: Overview of selected synthesis approaches for hierarchically structured zeolites, in terms of the textural control that they allow for.

		Control over:		
	Obtainable Pore Sizes	**Pore Size**	**Pore Connectivity**	**Porosity**
Bottom-Up Approaches				
Hard-Templating	Meso/Macropores	High	Limited	High
Soft-Templating	Mesopores	High	Medium	Limited
Non-Templating	Mesopores	Medium	Medium	Depends
Top-Down Approaches				
Demetallation	Mesopores, Hollow Crystals	Medium	Limited	High
Delamination	Mesopores	Medium	Limited	Medium
Surfactant assisted meso-structuring	Mesopores	High	Medium	Medium

The ability to control and tune the hierarchical pore network, together with the microstructure (which relates to the intrinsic kinetics), while keeping practical requirements in mind for production and use at scale, should be the focus of future research to synthesize zeolites with optimal properties for a given reaction. Another limitation of most presented synthesis methods is the obtained pore size. Most techniques aim to synthesize zeolite materials with controlled, small mesopores, while only a limited number of methods is able to realize controlled macropores or larger mesopores, in which diffusion is less restricted and capillary condensation of vapors may be preventable. On the other hand, as discussed in Section 3, the guidance provided by computational optimization does not often dictate a very narrowly defined optimal meso- or macropore size distribution, but a minimum pore diameter, d_{opt}, and this is an advantage that is insufficiently appreciated by many material chemists, who aim to perfectly tune the pore and crystal sizes – this might matter in certain applications, e.g., in optics, but not usually in catalysis. The key characteristics are the optimal porosity, ε_{opt}, and a maximum or optimum crystal size, w_{opt}, to minimize the local diffusion limitations and control product selectivity at the crystal level, with a well-connected wide pore network of sufficiently wide pores (d_{opt}).

Combining different methods in sequence, such as a templating approach followed by a post-synthetic modification, can generate multimodal pore systems and allow better control over the hierarchical pore system. An example is the preparation of macroporous zeolites by using mesoporous silica spheres as a hard template and subsequent introduction of mesopores by desilication after synthesis to obtain a hierarchical zeolite with additional intracrystalline macro and mesopores.[119] This may be useful to realize better access to the micropores via intracrystalline mesopores, and tune the selectivity at the crystal level; it may also mitigate the effects of deactivation by coking.

Characterization of hierarchically structured zeolites is an important part of guided material optimization. The complexity of the additional pore system with features over many length scales, ranging from nm to μm, complicates the characterization of hierarchically structured zeolites. This usually requires a combination of different techniques. Mitchell et al.[120] recently published a comprehensive overview about the characterization of hierarchically structured zeolites.

4.4 Surface barriers and grain boundaries

For the optimization of hierarchically structured zeolites, the effect of external and internal diffusion barriers on the overall diffusion rate in zeolites and, therefore, on their catalytic behavior should be considered too. As these barriers reduce the transport rate, it seems logical to wish to reduce or remove their influence; however, the barriers could be an additional handle to control selectivity, as they are species dependent. While the origin and nature of these diffusion barriers are not yet fully understood, many studies indicate their existence, and some could demonstrate their effect on catalysis. In general, one distinguishes two different barriers, internal barriers affecting intracrystalline diffusion, and external barriers, which have an impact on uptake rates of molecules into the micropores from the bulk fluid.

4.4.1 Internal surface barriers

Internal surface barriers can be intracrystalline or intercrystalline. Intercrystalline barriers are caused by grain boundaries in polycrystalline particles consisting of aggregated nanocrystals. The negative impact of internal grain boundaries on the catalytic performance of zeolites was recently reported for the isomerization of n-heptane. By comparing polycrystalline and monocrystalline Pt/Beta catalysts, the authors could demonstrate a distinctly negative impact of the internal grain boundaries present in the polycrystalline sample on the catalyst performance.[6b] Intracrystalline diffusion barriers in single crystals can be caused by defects

within them or by interfaces of intergrown zeolites, which lead to a mismatch of the pore alignment.[121] PFG-NMR measurements have shown that the diffusivities of the same molecule in different samples of the same zeolite differed by a factor of two, clearly indicating the existence of intracrystalline resistances.[122] For zeolite X, stacking faults could be identified as a possible reason for internal diffusion barriers.[123]

4.4.2 External surface barriers

Proof for the existence of external surface barriers can be found in both diffusion measurements and catalytic investigations. PFG NMR experiments have shown molecular exchange rates below those estimated using intracrystalline diffusivities, thus pointing to the existence of surface barriers.[124] Kärger and co-workers showed the great potential of microimaging techniques to measure the impact of surface barriers on mass transfer in microporous materials. Gobin and co-workers could demonstrate that the rate-determining step in diffusion of aromatics through MFI zeolites is dependent on the crystal dimensions and, thus, on the external surface-to-volume ratio. The rate-limiting step for overall diffusion in larger crystals was intracrystalline diffusion. In contrast, overall diffusion in small crystals was limited by surface effects, indicating the existence of surface barriers.[125]

In general, it is necessary to reduce or eliminate both internal and external diffusion barriers or, at least, consider their impact when optimizing the pore system of a hierarchically structured zeolite. However, without the proper understanding of the origin and effect of these barriers, the optimization of hierarchical zeolites is impossible. Additional work is necessary to quantify the role of such barriers, aided by molecular simulations,[73a, 126] which will allow for their systematic implementation in optimization models, as surface barriers may influence the rate determining step in the overall transport and reaction process. In the future, microimaging using guest molecule monitoring in microporous materials by interference and infrared microscopy could be a useful tool to quantify the effect of surface barriers on

diffusion in hierarchically structured zeolites, comparing experiments with molecular simulation. This would form the basis for the optimal design of hierarchically structured zeolites that properly include all the elementary transport and reaction steps.

5. Conclusions and outlook

Zeolites are uniquely beautiful catalysts. Their high intrinsic activity for acid site catalysis, which can be combined with other catalytic functions, e.g., by adding metals, and the ability to vary their microporous structure, so as to tune molecular size- and configuration-dependent selectivity are remarkable. This combination explains the industrial importance of zeolite catalysts, especially as some of these architectures can be generated at quite low cost. Catalyst design and synthesis efforts have concentrated on expanding the range of accessible zeolites and related zeolitic materials, like silicon aluminophosphates (SAPOs).

However, as in nature, catalysis at the nanoscale cannot function effectively without proper design at larger scales as well. Transport limitations readily occur in zeolites, which is the price to pay for the narrow pores, where molecular transport rates are typically orders of magnitude below those in the bulk. Catalyst particle size cannot be changed at will, because of reactor application requirements, for example related to pressure drop in fixed beds or fluid mechanics in fluidized beds. To facilitate molecular transport, industrial zeolite-based catalyst particles and pellets include wide pore channels – mesopores and macropores. This additional porosity is typically empirically determined, and it may even be a side effect of processes to alter the intrinsic activity, as in dealumination, creating extra-framework Al. It is no wonder that this creates poorly controlled porosity that is not optimally connected and may not effectively contribute to transport.

Since the 1990s, increasingly sophisticated methods have been proposed to generate mesopores, and, in some cases (but much less), macropores with controlled pore size. Bottom-up methods usually use sacrificial templates, although there are promising, non-templating-

based methods. The methods using sacrificial hard templates tend to be expensive, but macropores can be included more easily than with soft templates, which create mesopores, in some cases using templates that are either cheap enough or could be extracted and recycled. In some of these techniques, the zeolite crystal size can be controlled as well, down to the creation of nanocrystals, even assemblies of single nanosheets. In non-templating methods, control of the precise pore size is more difficult. The control over geometry, while preserving or imposing a desired Si/Al ratio, distribution and strength of acid sites, is not trivial. Top-down approaches, such as dealumination, desilication and delamination tend to affect both, although they are some of the most practiced, easiest and economically accessible techniques, building on long experience that can achieve some of the best results known to date. This expanding repertoire of bottom-up and top-down synthesis techniques begs the question which are the ones best suited to realize optimal catalyst designs, and which textural parameters should be aimed for?

Indeed, despite the wonderful chemistries and the beauty of some of the architectures generated using those techniques, how do such methods address the underlying questions on overall zeolite performance? Cost alone would make many methods inaccessible to industrial practice, however, are they even addressing the most pertinent issues – the parameters that have a primary effect on the overall catalyst yields, selectivity and stability?

This is where computational modeling is crucial. Methods were reviewed, including continuum and pore network models, to describe diffusion and reaction in hierarchically structured zeolites. For multiphase processes or those where deactivation may lead to significant changes in pore connectivity, network models should be employed to describe transport and reaction; otherwise, continuum models generally suffice.

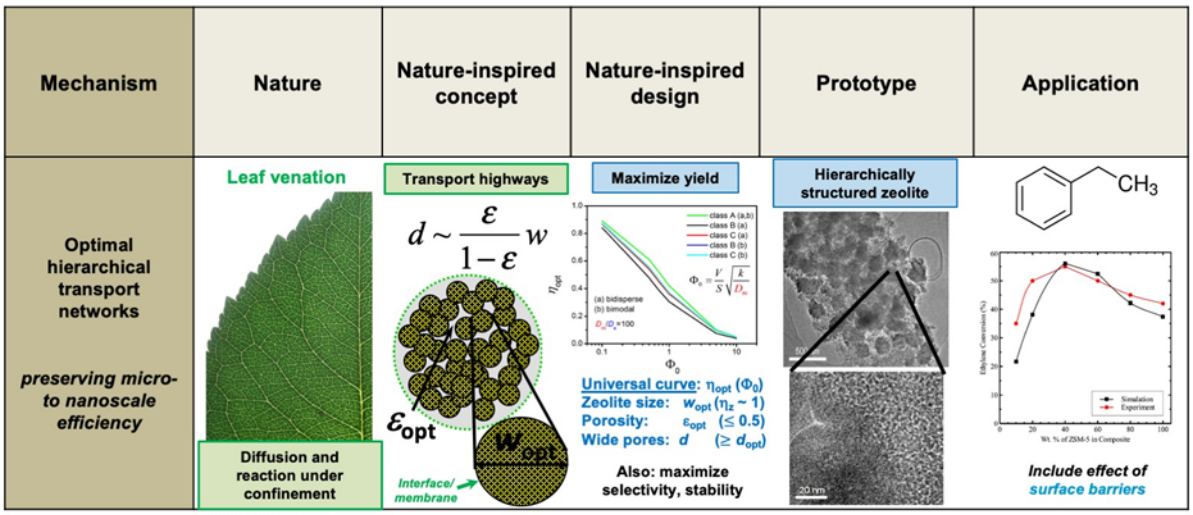

Figure 18: Nature-inspired engineering of hierarchically structured zeolites. Inspired by leaf venation and optimized by computation, an optimal distribution of uniform "highways" (wide mesopores or macropores) maximizes the yield in a catalyst particle or pellet. The effectiveness factor in the zeolite crystals, η_z, approaches 1, by using a maximum crystal size, w_{opt}. The precise distribution of the wide pore size, *d*, is of only secondary importance in the design of the additional porosity, but the value of the porosity, ε_{opt}, is crucial. The effectiveness factor in the optimal hierarchical catalyst, η_{opt}, follows a universal graph as a function of a modified Thiele modulus, Φ_0, which can be readily calculated from the reaction kinetics and the molecular diffusivity in the wide pores. Similarly, product selectivity can be tuned, and catalyst stability against deactivation can be maximized. Such nature-inspired design informs the synthesis, which can be realized using an increasing array of top-down and bottom-up techniques. The illustrated application is for ethylation of benzene, where also surface barriers play a role – as in nature, where interfaces crucially control transport in and out of reaction zones.

Whichever method is used to account for the wider pore channels, a multiscale modeling methodology is advocated for the catalyst pellet as a whole. This allows to address the specifics of intracrystalline configurational diffusion, which may require statistical mechanical techniques (like molecular dynamics and kinetic Monte-Carlo simulations), and the microkinetics of zeolite catalysis itself, underpinned by *ab initio*, quantum chemical methods. Without such multiscale methods, too much information is hidden in the effective diffusivity with a "tortuosity factor" that lumps a wide range of effects, from pore constructions and pore size distribution to pore connectivity. The impact of these effects can

depend on operation conditions and could vary over time. Such methods are unsuited for rational design.

Interestingly, despite the variety in hierarchical pore network structures, some useful general conclusions could be drawn. To get us there, inspiration from nature has been particularly useful. The computationally assisted, nature-inspired solution methodology, as applied to hierarchically structured zeolite design and synthesis, is summarized in Figure 18.

In nature, fractal architectures at larger length scales, where pressure-driven flow dominates, transition into uniform channel architectures at intermediate to small scales, where diffusion controls transport, down to the cells where reactions occur. This is observed in trees, the lungs, the vascular network and other crucial transport networks that link the micro- and the macroscale in a scalable and highly efficient way. Rather than being dogmatic about such structures being optimal, let alone optimal when translated to zeolite catalysis and reaction engineering, computational optimization has allowed us to extract general principles. Indeed, a Peclet number, $Pe \sim 1$, associated to the transition between convective and diffusive transport, has been shown to correspond to the transition from fractal to uniform architectures in nature – importantly, it also results from computational optimization. At a catalyst pellet level, the optimal wide pore channel architecture that maximally preserves function at the nanoscale, optimizing overall, observed yields for particles of a given size, is uniform, with pore diameters that are such that bulk molecular diffusion prevails. Between such wide pore channels of diameter, d_{opt}, are the nanoporous domains, here zeolite crystals, where the reactions occur at controlled conditions, preserving the desired selectivity and product distribution. To maximize yield, the local effectiveness factor in those zeolite nano- to microcrystals should be 1; some variation is possible, but the crystals should not be larger than a critical size, w_{opt}, where transport limitations within them would start to occur. Of course, this principle could be realized by a variety of methods: intercrystalline pores between

small crystals, or intracrystalline pores with thin enough crystalline zones in between the channels. It should be noted that zeolite-based composites, properly diluted or enhanced by a complementary catalytic function (as in FCC) may well realize the same effect. Similar to preserving the function and operation of cells in nature, the zeolite crystal function is preserved in such hierarchically structured zeolites.

As a guiding principle, the zeolite crystals should be sized such that there are no diffusion limitations inside them, or that diffusion is such that there is "molecular traffic control" intimately integrated with the catalytic function and leading to a desired product distribution – after all, selectivity is often the key outcome in catalysis, even more so than overall activity on a particle basis. Computations show that wide pores do not necessarily need to be finely tuned mesopores; in fact, macropores are often desired, especially for gas phase reactions, where Knudsen diffusion might further limit the transport rate when the mesopores are too narrow. The overall, added porosity occupied by those wide pores is crucial to maximize catalyst performance, and a simple analytical methodology, typically requiring no explicit solution of differential equations, was summarized here to determine its value, ε_{opt}, which is always at most 0.5. Too high, and space is wasted that could have been occupied by a productive zeolite; too low, and significant diffusion limitations will emerge. In addition, proper connectivity between the pores safeguards the catalyst against rapid catalyst deactivation, providing alternative pathways when some pores are obstructed. This value of ε_{opt}, together with the optimal (or at least, maximal) crystallite or crystal domain size, w_{opt}, determines the optimal (or at least, minimal) pore diameter d_{opt}. The distribution around this optimal pore diameter, d_{opt}, is only of secondary importance. Even a theoretical optimization of a pellet with concentric zones with different pore diameters shows little or no effect beyond

that which could be obtained using a uniform (ε_{opt}, w_{opt}, d_{opt}) combination, thus need not be a prime design target in hierarchically structured zeolite synthesis.

An emergent insight is the importance of both external and internal surface barriers in transport in (poly)crystalline zeolites, which may dominate the observed overall performance of zeolite catalysts. The barriers will also differ for adsorption and desorption processes. The presence of such barriers has long been suspected, underscored by molecular simulations and more recently elegantly demonstrated, using microimaging and spectroscopy. The origin of these barriers is still under debate and is unlikely to be a single source, valid for all zeolite-molecule combinations: free energy barriers have an enthalpic and an entropic contribution, and both may be influenced by the details of the surface structure. This structure may be affected (and thus possibly controlled) by a different chemistry and geometry at the nanoscale, induced by surface modifications and crystalline or amorphous layer addition or removal. This is an exciting avenue to control individual zeolite crystal and crystal aggregate performance. It also points to the possibility to tune this surface in overall hierarchical structural optimization, and to include it in computer models. That, of course, requires better understanding of surface barriers, prompting further research.

Again, this brings us back to nature: not just intracellular processes and the transport highways bridging cells, organs and organisms, but also the *interfaces* play a significant role. Could this not give us clues on the best architectures that explicitly include *designed interfaces* in and around zeolite crystals? Membranes are underpinning almost all molecular separation processes in living organisms, and some of them are remarkably selective, robust and permeable for the desired molecular or ionic species. Thus, we posit that zeolite surface barriers are an opportunity for design and process intensification, combining nanoscale membrane separation and intracrystalline reaction with optimized meso-macroporous diffusion networks. This endeavor will require refocusing synthesis efforts and computational

efforts to specifically include the surface barrier or interfacial, "skin" effect, as it may be a powerful handle to control overall zeolite catalyst activity, selectivity and stability.

Acknowledgements

MOC gratefully acknowledges support from the EPSRC via "Frontier Engineering" and "Frontier Engineering: Progression" Awards (EP/K038656/1, EP/S03305X/1).

Received: ((will be filled in by the editorial staff))
Revised: ((will be filled in by the editorial staff))
Published online: ((will be filled in by the editorial staff))

References

[1] B. B. Mandelbrot, *The Fractal Geometry of Nature*, 2 ed., Freeman, San Francisco, **1983**.
[2] M.-O. Coppens, *Industrial & Engineering Chemistry Research* **2005**, *44*, 5011-5019.
[3] aM.-O. Coppens, G. Ye, in *Diffusive Spreading in Nature, Technology and Society*, Springer, **2018**, pp. 203-232; bP. Trogadas, M. M. Nigra, M.-O. Coppens, *New Journal of Chemistry* **2016**, *40*, 4016-4026.
[4] aS. Li, J. Li, M. Dong, S. Fan, T. Zhao, J. Wang, W. Fan, *Chemical Society Reviews* **2019**, *48*, 885-907; bS. Mintova, M. Jaber, V. Valtchev, *Chemical Society Reviews* **2015**, *44*, 7207-7233; cJ. Přech, P. Pizarro, D. P. Serrano, J. Čejka, *Chemical Society Reviews* **2018**, *47*, 8263-8306; dW. Schwieger, A. G. Machoke, T. Weissenberger, A. Inayat, T. Selvam, M. Klumpp, A. Inayat, *Chemical Society Reviews* **2016**, *45*, 3353-3376.
[5] aE. Geus, J. Jansen, H. Van Bekkum, *Zeolites* **1994**, *14*, 82-88; bO. Geier, S. Vasenkov, E. Lehmann, J. Kärger, U. Schemmert, R. Rakoczy, J. Weitkamp, *The Journal of Physical Chemistry B* **2001**, *105*, 10217-10222; cJ. C. Saint Remi, A. Lauerer, C. Chmelik, I. Vandendael, H. Terryn, G. V. Baron, J. F. Denayer, J. Kärger, *Nature Materials* **2016**, *15*, 401-406.
[6] aS. M. Rao, E. Saraçi, R. Gläser, M.-O. Coppens, *Chemical Engineering Journal* **2017**, *329*, 45-55; bZ. Guo, X. Li, S. Hu, G. Ye, X. Zhou, M. O. Coppens, *Angewandte Chemie International Edition* **2020**, *132*, 1564-1567.
[7] M.-O. Coppens, *Current Opinion in Chemical Engineering* **2012**, *1*, 281-289.
[8] R. Metzler, J. Klafter, *Physics Reports* **2000**, *339*, 1-77.
[9] aM.-O. Coppens, A. T. Bell, A. K. Chakraborty, *Chemical Engineering Science* **1998**, *53*, 2053-2061; bC. Ball, N. MacWilliam, J. K. Percus, R. K. Bowles, *The Journal of Chemical Physics* **2009**, *130*, 054504; cP. Demontis, G. Stara, G. B. Suffritti, *Microporous and Mesoporous Materials* **2005**, *86*, 166-175; dI. M. Sokolov, *Soft Matter* **2012**, *8*, 9043-9052; eP. M. Richards, *Physical Review B* **1977**, *16*, 1393.
[10] aK. Allen, T. Von Backström, D. Kröger, *Powder Technology* **2013**, *246*, 590-600; bD. Wu, J. Zhou, Y. Li, *AIChE Journal* **2007**, *53*, 2618-2629.
[11] aG. Baron, M. Van de Voorde, H. Verelst, P. Jacobs, J. Martens, in *Studies in Surface Science and Catalysis, Vol. 80*, Elsevier, **1993**, pp. 45-49; bT. N. Linh, H. Fujita, A. Sakoda, *Adsorption* **2016**, *22*, 1001-1011; cD. M. Ruthven, in *Studies in Surface*

Science and Catalysis, Vol. 97, Elsevier, **1995**, pp. 223-234; dY. Nakasaka, T. Kanda, K.-i. Shimizu, K. Kon, G. Shibata, T. Masuda, *Catalysis Today* **2019**, *332*, 64-68.
[12] aC.-C. Chang, A. R. Teixeira, C. Li, P. J. Dauenhauer, W. Fan, *Langmuir* **2013**, *29*, 13943-13950; bP. Bai, E. Haldoupis, P. J. Dauenhauer, M. Tsapatsis, J. I. Siepmann, *ACS Nano* **2016**, *10*, 7612-7618.
[13] G. F. Froment, K. B. Bischoff, J. De Wilde, *Chemical Reactor Analysis and Design*, 3 ed., Wiley, New York, **2010**.
[14] G. Ye, Y. Sun, Z. Guo, K. Zhu, H. Liu, X. Zhou, M.-O. Coppens, *Journal of Catalysis* **2018**, *360*, 152-159.
[15] C. Fernandez, I. Stan, J. P. Gilson, K. Thomas, A. Vicente, A. Bonilla, J. Pérez-Ramírez, *Chemistry–A European Journal* **2010**, *16*, 6224-6233.
[16] aA. Wheeler, in *Advances in Catalysis, Vol. 3*, Elsevier, **1951**, pp. 249-327; bM.-O. Coppens, in *Structured Catalysts and Reactors*, 2 ed., Taylor and Francis, New York, **2005**, pp. 779-805.
[17] J. Weitkamp, S. Ernst, L. Puppe, in *Catalysis and Zeolites*, Springer, **1999**, pp. 327-376.
[18] N. Chen, W. Kaeding, F. Dwyer, *Journal of the American Chemical Society* **1979**, *101*, 6783-6784.
[19] J. A. Moulijn, A. Van Diepen, F. Kapteijn, *Applied Catalysis A: General* **2001**, *212*, 3-16.
[20] aG. Froment, *Catalysis Reviews* **2008**, *50*, 1-18; bG. Froment, *Applied Catalysis A: General* **2001**, *212*, 117-128.
[21] Y. H. Kim, K. H. Lee, C. M. Nam, J. S. Lee, *ChemCatChem* **2012**, *4*, 1143-1153.
[22] aF. J. Keil, *Catalysis Today* **1999**, *53*, 245-258; bF. J. Keil, *Modeling and Simulation of Heterogeneous Catalytic Reactions: From the Molecular Process to the Technical System* **2011**, 149-186.
[23] B. E. Poling, J. M. Prausnitz, J. P. O'Connell, *The Properties of Gases and Liquids*, 5 ed., McGraw-Hill, New York, **2001**.
[24] R. Krishna, J. Wesselingh, *Chemical Engineering Science* **1997**, *52*, 861-911.
[25] W. Pollard, R. D. Present, *Physical Review* **1948**, *73*, 762-774.
[26] aJ. Kaerger, *ChemPhysChem* **2015**, *16*, 24-51; bJ. Kärger, D. M. Ruthven, D. N. Theodorou, *Diffusion in Nanoporous Materials*, John Wiley & Sons, **2012**.
[27] P. Weisz, *Chemtech* **1973**, 498-505.
[28] aS. C. Reyes, J. H. Sinfelt, G. J. DeMartin, *the Journal of Physical Chemistry B* **2000**, *104*, 5750-5761; bJ. M. Zalc, S. C. Reyes, E. Iglesia, *Chemical Engineering Science* **2003**, *58*, 4605-4617.
[29] J. Kärger, H. Pfeifer, *Zeolites* **1987**, *7*, 90-107.
[30] M.-O. Coppens, A. T. Bell, A. K. Chakraborty, *Chemical Engineering Science* **1999**, *54*, 3455-3463.
[31] R. Krishna, J. Van Baten, *Chemical Physics Letters* **2005**, *407*, 159-165.
[32] aP. Kortunov, L. Heinke, S. Vasenkov, C. Chmelik, D. B. Shah, J. Kärger, R. A. Rakoczy, Y. Traa, J. Weitkamp, *The Journal of Physical Chemistry B* **2006**, *110*, 23821-23828; bS. Vasenkov, W. Böhlmann, P. Galvosas, O. Geier, H. Liu, J. Kärger, *The Journal of Physical Chemistry B* **2001**, *105*, 5922-5927; cP. Kortunov, S. Vasenkov, C. Chmelik, J. Kärger, D. M. Ruthven, J. Wloch, *Chemistry of Materials* **2004**, *16*, 3552-3558.
[33] J. Cejka, A. Corma, S. Zones, *Zeolites and Catalysis: Synthesis, Reactions and Applications*, John Wiley & Sons, **2010**.
[34] M. Sahimi, G. R. Gavalas, T. T. Tsotsis, *Chemical Engineering Science* **1990**, *45*, 1443-1502.
[35] N. Epstein, *Chemical Engineering Science* **1989**, *44*, 777-779.

[36] aN. Wakao, J. Smith, *Industrial & Engineering Chemistry Fundamentals* **1964**, *3*, 123-127; bN. Wakao, J. Smith, *Chemical Engineering Science* **1962**, *17*, 825-834.
[37] J. Szekely, J. Evans, *Chemical Engineering Science* **1970**, *25*, 1091-1107.
[38] G. Ye, Y. Sun, X. Zhou, K. Zhu, J. Zhou, M.-O. Coppens, *Chemical Engineering Journal* **2017**, *329*, 56-65.
[39] aG. Ye, H. Wang, X. Duan, Z. Sui, X. Zhou, M. O. Coppens, W. Yuan, *AIChE Journal* **2019**, *65*, 140-150; bG. Ye, H. Wang, X. Zhou, F. J. Keil, M. O. Coppens, W. Yuan, *AIChE Journal* **2019**, *65*, e16687; cG. Ye, X. Zhou, J. Zhou, W. Yuan, M. O. Coppens, *AIChE Journal* **2017**, *63*, 78-86; dG. Ye, X. Zhou, W. Yuan, M. O. Coppens, *AIChE Journal* **2016**, *62*, 451-460; eJ. Wood, L. Gladden, *Chemical Engineering Science* **2002**, *57*, 3033-3045; fJ. Wood, L. Gladden, F. Keil, *Chemical Engineering Science* **2002**, *57*, 3047-3059.
[40] aF. Larachi, R. Hannaoui, P. Horgue, F. Augier, Y. Haroun, S. Youssef, E. Rosenberg, M. Prat, M. Quintard, *Chemical Engineering Journal* **2014**, *240*, 290-306; bV. Novák, F. Štěpánek, P. Kočí, M. Marek, M. Kubíček, *Chemical Engineering Science* **2010**, *65*, 2352-2360.
[41] C. A. Baldwin, A. J. Sederman, M. D. Mantle, P. Alexander, L. F. Gladden, *Journal of Colloid and Interface Science* **1996**, *181*, 79-92.
[42] aJ.-Y. Arns, V. Robins, A. P. Sheppard, R. M. Sok, W. V. Pinczewski, M. A. Knackstedt, *Transport in Porous media* **2004**, *55*, 21-46; bR. Al-Raoush, K. Thompson, C. S. Willson, *Soil Science Society of America Journal* **2003**, *67*, 1687-1700.
[43] aH. Dong, M. J. Blunt, *Physical Review E* **2009**, *80*, 036307; bD. Silin, T. Patzek, *Physica A: Statistical mechanics and its applications* **2006**, *371*, 336-360.
[44] aP. Sharratt, R. Mann, *Chemical Engineering Science* **1987**, *42*, 1565-1576; bM. Hollewand, L. Gladden, *Chemical Engineering Science* **1992**, *47*, 1761-1770.
[45] M. Hollewand, L. Gladden, *Chemical Engineering Science* **1992**, *47*, 2757-2762.
[46] M.-O. Coppens, *Catalysis Today* **1999**, *53*, 225-243.
[47] aB. O'Regan, M. Grätzel, *Nature* **1991**, *353*, 737-740; bD. K. Dogutan, D. G. Nocera, *Accounts of Chemical Research* **2019**, *52*, 3143-3148; cS. Berardi, S. Drouet, L. Francàs, C. Gimbert-Suriñach, M. Guttentag, C. Richmond, T. Stoll, A. Llobet, *Chemical Society Reviews* **2014**, *43*, 7501-7519; dD. Gust, T. A. Moore, A. L. Moore, *Accounts of Chemical Research* **2009**, *42*, 1890-1898; eP. Trogadas, M.-O. Coppens, *Chemical Society Reviews* **2020**, *49*, 3107-3141.
[48] V. Vecchi, S. Barera, R. Bassi, L. Dall'Osto, *Plants* **2020**, *9*, 67.
[49] A. S. Perera, M.-O. Coppens, *Philosophical Transactions of the Royal Society A* **2019**, *377*, 20180268.
[50] M. M. Kearney, *Chemical Engineering Progress* **2000**, *96*, 61-68.
[51] D. Christensen, J. Nijenhuis, J. van Ommen, M.-O. Coppens, *Industrial & Engineering Chemistry Research* **2008**, *47*, 3601-3618.
[52] P. Trogadas, J. Cho, T. Neville, J. Marquis, B. Wu, D. Brett, M.-O. Coppens, *Energy & Environmental Science* **2018**, *11*, 136-143.
[53] S. Gheorghiu, S. Kjelstrup, P. Pfeifer, M.-O. Coppens, in *Fractals in Biology and Medicine*, Springer, **2005**, pp. 31-42.
[54] aC. Murray, *USA* **1926**, *12*, 207-213; bC. D. Murray, *Proceedings of the National Academy of Sciences of the United States of America* **1926**, *12*, 299.
[55] S. Vogel, *Journal of Biosciences* **2004**, *29*, 391-397.
[56] M. H. Chin, E. Gentleman, M.-O. Coppens, R. M. Day, *Trends in Biotechnology* **2020**, *38*, 1054-1065.

[57] aF. K. van Willigen, D. Christensen, J. Van Ommen, M.-O. Coppens, *Catalysis Today* **2005**, *105*, 560-568; bD. Christensen, D. Vervloet, J. Nijenhuis, B. Van Wachem, J. Van Ommen, M.-O. Coppens, *Powder Technology* **2008**, *183*, 454-466.
[58] L. Sack, C. Scoffoni, *New Phytologist* **2013**, *198*, 983-1000.
[59] P. Kortunov, S. Vasenkov, J. Kärger, M. Fé Elía, M. Perez, M. Stöcker, G. Papadopoulos, D. Theodorou, B. Drescher, G. McElhiney, *Chemistry of Materials* **2005**, *17*, 2466-2474.
[60] aN. Örs, T. Doğu, *AIChE Journal* **1979**, *25*, 723-725; bT. Doğu, *Industrial & Engineering Chemistry Research* **1998**, *37*, 2158-2171.
[61] M. Loewenberg, *The Journal of Chemical Physics* **1994**, *100*, 7580-7589.
[62] S. Gheorghiu, M.-O. Coppens, *AIChE Journal* **2004**, *50*, 812-820.
[63] G. Wang, E. Johannessen, C. R. Kleijn, S. W. de Leeuw, M.-O. Coppens, *Chemical Engineering Science* **2007**, *62*, 5110-5116.
[64] G. Ye, X. Duan, K. Zhu, X. Zhou, M.-O. Coppens, W. Yuan, *Chemical Engineering Science* **2015**, *132*, 108-117.
[65] E. Johannessen, G. Wang, M.-O. Coppens, *Industrial & Engineering Chemistry Research* **2007**, *46*, 4245-4256.
[66] G. Wang, M.-O. Coppens, *Industrial & Engineering Chemistry Research* **2008**, *47*, 3847-3855.
[67] G. Wang, M.-O. Coppens, *Chemical Engineering Science* **2010**, *65*, 2344-2351.
[68] X. Liu, H. Wang, G. Ye, X. Zhou, F. J. Keil, *Chemical Engineering Journal* **2019**, *373*, 1389-1396.
[69] aS. M. Rao, M.-O. Coppens, *Chemical Engineering Science* **2012**, *83*, 66-76; bS. M. Rao, M.-O. Coppens, *Industrial & Engineering Chemistry Research* **2010**, *49*, 11087-11097.
[70] Y. Shi, G. Ye, C. Yang, Y. Tang, C. Peng, G. Qian, W. Yuan, X. Duan, X. Zhou, *Chemical Engineering Science* **2019**, *202*, 336-346.
[71] F. J. Keil, C. Rieckmann, *Chemical Engineering Science* **1994**, *49*, 4811-4822.
[72] X. Liu, Q. Zhang, G. Ye, J. Li, P. Li, X. Zhou, F. J. Keil, *Chemical Engineering Science* **2020**, *211*, 115305.
[73] aF. J. Keil, R. Krishna, M.-O. Coppens, *Reviews in Chemical Engineering* **2000**, *16*, 71-197; bB. Smit, T. L. Maesen, *Chemical Reviews* **2008**, *108*, 4125-4184; cJ. S. Bhatt, A. Chutia, C. R. A. Catlow, M.-O. Coppens, in *Modern Developments in Catalysis*, World Scientific, **2017**, pp. 253-288.
[74] N. Hansen, R. Krishna, J. Van Baten, A. T. Bell, F. Keil, *The Journal of Physical Chemistry C* **2009**, *113*, 235-246.
[75] B. Vandegehuchte, I. R. Choudhury, J. Thybaut, J. Martens, G. Marin, *The Journal of Physical Chemistry C* **2014**, *118*, 22053-22068.
[76] H. Li, M. Ye, Z. Liu, *Chemical Engineering Science* **2016**, *147*, 1-12.
[77] W. Ding, H. Li, P. Pfeifer, R. Dittmeyer, *Chemical Engineering Journal* **2014**, *254*, 545-558.
[78] aD. Cai, H. Xiong, C. Zhang, F. Wei, *Small* **2020**, *16*, 1901979; bD. Cai, Y. Hou, C. Zhang, N. Wang, Z. Chen, W. Song, Z. Jia, Y. Wang, W. Qian, F. Wei, *Nanoscale* **2018**, *10*, 16431-16433.
[79] M. Gao, H. Li, W. Liu, Z. Xu, S. Peng, M. Yang, M. Ye, Z. Liu, *Nature communications* **2020**, *11*, 3641, pp. 1-11.
[80] aJ. Vernimmen, V. Meynen, P. Cool, *Beilstein Journal of Nanotechnology* **2011**, *2*, 785-801; bY. Wei, T. E. Parmentier, K. P. de Jong, J. Zečević, *Chemical Society Reviews* **2015**, *44*, 7234-7261.
[81] T. Weissenberger, B. Reiprich, A. G. F. Machoke, K. Klühspies, J. Bauer, R. Dotzel, J. L. Casci, W. Schwieger, *Catalysis Science & Technology* **2019**, *9*, 3259-3269.

[82] B. T. Holland, L. Abrams, A. Stein, *Journal of the American Chemical Society* **1999**, *121*, 4308-4309.
[83] T. Weissenberger, R. Leonhardt, B. A. Zubiri, M. Pitínová-Štekrová, T. L. Sheppard, B. Reiprich, J. Bauer, R. Dotzel, M. Kahnt, A. Schropp, C. G. Schroer, J.-D. Grunwaldt, J. L. Casci, J. Čejka, E. Spiecker, W. Schwieger, *Chemistry – A European Journal* **2019**, *25*, 14430-14440.
[84] aB. Gil, Ł. Mokrzycki, B. Sulikowski, Z. Olejniczak, S. Walas, *Catalysis Today* **2010**, *152*, 24-32; bM. Bjørgen, F. Joensen, M. Spangsberg Holm, U. Olsbye, K.-P. Lillerud, S. Svelle, *Applied Catalysis A: General* **2008**, *345*, 43-50.
[85] aS. Van Donk, A. H. Janssen, J. H. Bitter, K. P. de Jong, *Catalysis Reviews* **2003**, *45*, 297-319; bJ. Zečević, C. J. Gommes, H. Friedrich, P. E. de Jongh, K. P. de Jong, *Angewandte Chemie International Edition* **2012**, *51*, 4213-4217.
[86] M. Milina, S. Mitchell, P. Crivelli, D. Cooke, J. Pérez-Ramírez, *Nature Communications* **2014**, *5*, 1-10.
[87] A. H. Lu, F. Schüth, *Advanced Materials* **2006**, *18*, 1793-1805.
[88] N. Chu, J. Wang, Y. Zhang, J. Yang, J. Lu, D. Yin, *Chemistry of Materials* **2010**, *22*, 2757-2763.
[89] V. Valtchev, B. J. Schoeman, J. Hedlund, S. Mintova, J. Sterte, *Zeolites* **1996**, *17*, 408-415.
[90] C. Xue, T. Xu, J. Zheng, J. Wang, Z. Zhang, X. Hao, A. Abudula, G. Guan, *Materials Letters* **2015**, *154*, 55-59.
[91] B. Li, Z. Hu, B. Kong, J. Wang, W. Li, Z. Sun, X. Qian, Y. Yang, W. Shen, H. Xu, *Chemical Science* **2014**, *5*, 1565-1573.
[92] A. G. Machoke, A. M. Beltrán, A. Inayat, B. Winter, T. Weissenberger, N. Kruse, R. Güttel, E. Spiecker, W. Schwieger, *Advanced Materials* **2015**, *27*, 1066-1070.
[93] Y. Zhu, Z. Hua, J. Zhou, L. Wang, J. Zhao, Y. Gong, W. Wu, M. Ruan, J. Shi, *Chemistry–A European Journal* **2011**, *17*, 14618-14627.
[94] J. Jin, C. Peng, J. Wang, H. Liu, X. Gao, H. Liu, C. Xu, *Industrial & Engineering Chemistry Research* **2014**, *53*, 3406-3411.
[95] W. Park, D. Yu, K. Na, K. E. Jelfs, B. Slater, Y. Sakamoto, R. Ryoo, *Chemistry of Materials* **2011**, *23*, 5131-5137.
[96] M. Choi, K. Na, J. Kim, Y. Sakamoto, O. Terasaki, R. Ryoo, *Nature* **2009**, *461*, 246-249.
[97] R. J. Messinger, K. Na, Y. Seo, R. Ryoo, B. F. Chmelka, *Angewandte Chemie International Edition* **2015**, *54*, 927-931.
[98] K. Na, M. Choi, R. Ryoo, *Microporous and Mesoporous Materials* **2013**, *166*, 3-19.
[99] Z. Wang, C. Li, H. J. Cho, S.-C. Kung, M. A. Snyder, W. Fan, *Journal of Materials Chemistry A* **2015**, *3*, 1298-1305.
[100] A. Inayat, C. Schneider, W. Schwieger, *Chemical Communications* **2015**, *51*, 279-281.
[101] S. Ferdov, *Microporous and Mesoporous Materials* **2020**, *303*, 110263.
[102] B. Reiprich, T. Weissenberger, W. Schwieger, A. Inayat, *Frontiers of Chemical Science and Engineering* **2020**, *14*, 127-142.
[103] J. Wang, W. Yue, W. Zhou, M.-O. Coppens, *Microporous and Mesoporous Materials* **2009**, *120*, 19-28.
[104] J. Wang, J. C. Groen, W. Yue, W. Zhou, M.-O. Coppens, *Journal of Materials Chemistry* **2008**, *18*, 468-474.
[105] J. Wang, J. C. Groen, W. Yue, W. Zhou, M.-O. Coppens, *Chemical Communications* **2007**, *44*, 4653-4655.
[106] aH. Zhu, Z. Liu, Y. Wang, D. Kong, X. Yuan, Z. Xie, *Chemistry of Materials* **2008**, *20*, 1134-1139; bK. Na, M. Choi, W. Park, Y. Sakamoto, O. Terasaki, R. Ryoo, *Journal of the American Chemical Society* **2010**, *132*, 4169-4177.

[107] aD. Verboekend, S. Mitchell, M. Milina, J. C. Groen, J. Pérez-Ramírez, *The Journal of Physical Chemistry C* **2011**, *115*, 14193-14203; bD. Verboekend, J. Pérez-Ramírez, *Catalysis Science & Technology* **2011**, *1*, 879-890.
[108] D. Verboekend, J. Pérez-Ramírez, *Chemistry–A European Journal* **2011**, *17*, 1137-1147.
[109] aC. Dai, A. Zhang, L. Li, K. Hou, F. Ding, J. Li, D. Mu, C. Song, M. Liu, X. Guo, *Chemistry of Materials* **2013**, *25*, 4197-4205; bT. Li, J. Ihli, Z. Ma, F. Krumeich, J. A. van Bokhoven, *The Journal of Physical Chemistry C* **2019**, *123*, 8793-8801.
[110] W. J. Roth, P. Nachtigall, R. E. Morris, J. Cejka, *Chemical Reviews* **2014**, *114*, 4807-4837.
[111] aW. J. Roth, J. Čejka, *Catalysis Science & Technology* **2011**, *1*, 43-53; bA. Corma, V. Fornes, J. Martınez-Triguero, S. Pergher, *Journal of Catalysis* **1999**, *186*, 57-63.
[112] J. García-Martínez, M. Johnson, J. Valla, K. Li, J. Y. Ying, *Catalysis Science & Technology* **2012**, *2*, 987-994.
[113] J. García-Martínez, K. Li, G. Krishnaiah, *Chemical Communications* **2012**, *48*, 11841-11843.
[114] H. I. Lee, H. J. Park, Y.-K. Park, J. Y. Hur, J.-K. Jeon, J. M. Kim, *Catalysis Today* **2008**, *132*, 68-74.
[115] I. I. Ivanova, E. E. Knyazeva, *Chemical Society Reviews* **2013**, *42*, 3671-3688.
[116] aD. Verboekend, J. Pérez-Ramírez, *Chemistry – A European Journal* **2011**, *17*, 1137-1147; bZ. Qin, L. Lakiss, J.-P. Gilson, K. Thomas, J.-M. Goupil, C. Fernandez, V. Valtchev, *Chemistry of Materials* **2013**, *25*, 2759-2766; cI. Ogino, M. M. Nigra, S.-J. Hwang, J.-M. Ha, T. Rea, S. I. Zones, A. Katz, *Journal of the American Chemical Society* **2011**, *133*, 3288-3291; dS. Maheshwari, E. Jordan, S. Kumar, F. S. Bates, R. L. Penn, D. F. Shantz, M. Tsapatsis, *Journal of the American Chemical Society* **2008**, *130*, 1507-1516; eJ. Garcia-Martinez, M. Johnson, J. Valla, K. Li, J. Y. Ying, *Catalysis Science & Technology* **2012**, *2*, 987-994; fS. Inagaki, M. Ogura, T. Inami, Y. Sasaki, E. Kikuchi, M. Matsukata, *Microporous and Mesoporous Materials* **2004**, *74*, 163-170.
[117] J. Čejka, R. Millini, M. Opanasenko, D. P. Serrano, W. J. Roth, *Catalysis Today* **2020**, *345*, 2-13.
[118] R. Chal, C. Gérardin, M. Bulut, S. Van Donk, *ChemCatChem* **2011**, *3*, 67-81.
[119] T. Weissenberger, A. G. F. Machoke, J. Bauer, R. Dotzel, J. L. Casci, M. Hartmann, W. Schwieger, *ChemCatChem* **2020**, *12 (9)*, 2461-2468.
[120] S. Mitchell, A. B. Pinar, J. Kenvin, P. Crivelli, J. Kärger, J. Pérez-Ramírez, *Nature Communications* **2015**, *6*, 1-14.
[121] L. Karwacki, M. H. Kox, D. M. De Winter, M. R. Drury, J. D. Meeldijk, E. Stavitski, W. Schmidt, M. Mertens, P. Cubillas, N. John, *Nature Materials* **2009**, *8*, 959-965.
[122] K. Ulrich, D. Freude, P. Galvosas, C. Krause, J. Kärger, J. Caro, P. Poladli, H. Papp, *Microporous and Mesoporous Materials* **2009**, *120*, 98-103.
[123] A. Feldhoff, J. Caro, H. Jobic, J. Ollivier, C. B. Krause, P. Galvosas, J. Kärger, *ChemPhysChem* **2009**, *10*, 2429-2433.
[124] aM. B. J. Caro, H. Jobic, J. Kärger, B. Zibrowius, *Advances in Catalysis* **1993**, *39*, 351-414; bJ. Kärger, M. Bülow, G. R. Millward, J. M. Thomas, *Zeolites* **1986**, *6*, 146-150.
[125] O. Gobin, S. Reitmeier, A. Jentys, J. Lercher, *The Journal of Physical Chemistry C* **2009**, *113*, 20435-20444.
[126] D. A. Newsome, D. S. Sholl, *The Journal of Physical Chemistry B* **2005**, *109*, 7237-7244.